Monthly Notices
of the
ROYAL ASTRONOMICAL SOCIETY

MNRAS **464,** 2174–2202 (2017)
Advance Access publication 2016 October 3

doi:10.1093/mnras/stw2488

N-body modelling of globular clusters: masses, mass-to-light ratios and intermediate-mass black holes

H. Baumgardt★

School of Mathematics and Physics, The University of Queensland, St. Lucia, QLD 4072, Australia

Accepted 2016 September 29. Received 2016 September 27; in original form 2016 May 13; Editorial Decision 2016 September 27

ABSTRACT

We have determined the masses and mass-to-light ratios of 50 Galactic globular clusters by comparing their velocity dispersion and surface brightness profiles against a large grid of 900 *N*-body simulations of star clusters of varying initial concentration, size and central black hole mass fraction. Our models follow the evolution of the clusters under the combined effects of stellar evolution and two-body relaxation allowing us to take the effects of mass segregation and energy equipartition between stars self-consistently into account. For a subset of 16 well-observed clusters, we also derive their kinematic distances. We find an average mass-to-light ratio of Galactic globular clusters of $<M/L_V> = 1.98 \pm 0.03$, which agrees very well with the expected M/L ratio if the initial mass function (IMF) of the clusters was a standard Kroupa or Chabrier mass function. We do not find evidence for a decrease in the average mass-to-light ratio with metallicity. The surface brightness and velocity dispersion profiles of most globular clusters are incompatible with the presence of intermediate-mass black holes (IMBHs) with more than a few thousand $M_\odot$ in them. The only clear exception is ω Cen, where the velocity dispersion profile provides strong evidence for the presence of a $\sim$40 000 $M_\odot$ IMBH in the centre of the cluster.

Key words: stars: luminosity function, mass function – globular clusters: general – globular clusters: individual: ω Cen.

1 INTRODUCTION

Globular clusters (GCs) are among the oldest structures in the Universe, having formed within 1 to 2 Gyr after the big bang (Kravtsov & Gnedin 2005). Studying their origin and evolution has therefore important implications for our understanding of star formation and the growth of structure in the early Universe. In addition, due to their high central densities and high stellar encounter rates, GCs are also unique environments for the creation of exotic stars like blue stragglers (Bailyn 1995; Davies, Piotto & de Angeli 2004), low-mass X-ray binaries (Verbunt 1993; Pooley et al. 2003) and millisecond pulsars (Manchester et al. 1991). The high stellar densities in GCs could also give rise to the creation of intermediate-mass black holes (IMBHs; Portegies Zwart & McMillan 2002; Portegies Zwart et al. 2004; Giersz et al. 2015), which might be the progenitors of supermassive black holes in galactic centres. Finally, GCs are important environments for the creation of tight black hole binaries which merge through the emission of gravitational waves (Banerjee, Baumgardt & Kroupa 2010; Downing et al. 2011; Askar et al. 2017; Rodriguez, Chatterjee & Rasio 2016a; Rodriguez et al. 2016b).

In order to understand the rate of creation of exotic stars, it is important to know the mass density profile of GCs and how different types of stars are distributed within a GC. This is possible by a detailed modelling of the internal kinematics of GCs. Several methods have been suggested in the literature to derive cluster masses from observed density profiles: one can either use analytic formulas which relate a cluster's mass to its radius and velocity dispersion inside some radius (e.g. Mandushev, Staneva & Spasova 1991; Strader, Caldwell & Seth 2011), or fit analytic density profiles like Plummer or King models to the observed velocity and surface density profiles of GCs (e.g. McLaughlin & van der Marel 2005; Kimmig et al. 2015). Finally, it is possible to deproject the observed surface density profile and then derive the cluster mass through Jeans modelling and a fit of the observed velocity dispersion profile (e.g. van de Ven et al. 2006; Noyola, Gebhardt & Bergmann 2008; Lützgendorf et al. 2012, 2013b).

Most approaches assume a constant mass-to-light ratio inside GCs. However, since the relaxation times of GCs are generally much smaller than their ages, high-mass stars like compact remnants and giant stars are concentrated towards the cluster centres, while low-mass stars are pushed towards the outer cluster parts (Baumgardt & Makino 2003). Hence the assumption of a constant mass-to-light ratio is not valid for GCs. In addition, due to energy equipartition, massive stars move more slowly at a given radius compared to

★ E-mail: h.baumgardt@uq.edu.au

average cluster stars (Trenti & van der Marel 2013; Bianchini et al. 2016). As a result, the velocity dispersion derived from giant stars will underestimate the true velocity dispersion, which leads to an underestimation of the total cluster mass if mass segregation is not properly taken into account (Shanahan & Gieles 2015).

It is possible to account for mass segregation by e.g. using multimass King–Michie models (Michie 1963; Gunn & Griffin 1979) or the more recently suggested LIMEPY models (Gieles & Zocchi 2015; Zocchi et al. 2016b). Multimass models have however additional degrees of freedom since the amount of mass segregation between different mass components can in principle be freely chosen in the models.

In this paper, we follow a different approach to derive the absolute masses and mass-to-light ratios of GCs from their surface density and velocity dispersion profiles. We perform a large grid of *N*-body simulations and scale each model so that it has the same half-light radius as the observed clusters. Scaling is done in such a way that the relaxation time is kept constant, thereby making sure that mass segregation of stars and (partial) energy equipartition between them are taken into account in a self-consistent way in the scaled models, i.e. each model has the exact amount of mass segregation which a real GC would have if it started from the same initial condition. We then determine the model which best fits the observed density and velocity dispersion profile for each GC and determine the total mass, mass-to-light ratio and the possible presence of an IMBH in the observed clusters from the best-fitting model. Our paper is organized as follows: in Section 2, we describe the grid of *N*-body models that we have performed, and in Section 3, we describe the selection of the observational data. Section 4 presents our results and we draw our conclusions in Section 5.

2 THE *N*-BODY MODELS

In total, we calculated a grid of ∼900 *N*-body simulations, varying the initial density profile, half-mass radius $r_{\rm h}$, cluster metallicity [Fe/H] and the mass fraction $M_{\rm BH}/M_{\rm GC}$ of a central IMBH between the different simulations. Our clusters did not contain primordial binaries, however binaries could form dynamically during the simulations. All the simulations were made using the GPU-enabled version of the collisional *N*-body code NBODY6 (Aarseth 1999; Nitadori & Aarseth 2012). The clusters without IMBHs and the clusters with IMBH mass fractions of $M_{\rm BH}/M_{\rm GC} = 0.01$ and $M_{\rm BH}/M_{\rm GC} = 0.02$ started with $N = 100\,000$ stars, while the clusters with an IMBH mass fraction of $M_{\rm BH}/M_{\rm GC} = 0.005$ were run with $N = 200\,000$ stars initially. In total, we performed 720 simulations with $N = 100\,000$ stars and 48 simulations with $N = 200\,000$ stars. We also performed test simulations with $N = 50\,000$ stars to test the dependence of our results on the initial number of cluster stars, but found that the initial particle number has a negligible influence on the results.

The initial density profiles of our clusters were given by King (1962) models with initial dimensionless central concentrations of $c = \log r_{\rm c}/r_{\rm t}$ of c =0.2, 0.5, 1.0, 1.5, 2.0 and 2.5, respectively. We also simulated clusters starting with King (1966) density profiles, but found that these led to clusters with too small a variation in the final density profile which cannot fit the observed surface density profiles for a significant fraction of GCs. Initial cluster models were set up using the method described in Hilker et al. (2007), by first deprojecting the density profile, then calculating the distribution function $f(E)$ and finally choosing particle positions and velocities. We used eight grid points for the initial half-mass radius $r_{\rm h}$ given by $r_{\rm h}$ = 2, 3, 5, 7, 10, 15, 25 and 35 pc for the $N = 50\,000$ star clusters. For the $N = 100\,000$ and $N = 200\,000$ star clusters, the initial half-mass radii were reduced by factors of 0.836 and 0.696, respectively, so that these clusters have the same initial relaxation time as the corresponding $N = 50\,000$ star models. For each value of $r_{\rm h}$ and c, we ran three simulations starting from different random number seeds to increase the statistical significance of our results.

Stellar evolution was modelled according to the stellar evolution routines of Hurley, Pols & Tout (2000), assuming black hole and neutron star retention fractions of 10 per cent. All clusters started with stars distributed according to a Kroupa (2001) mass function with lower and upper mass limits of 0.1 $M_\odot$ and 100 $M_\odot$, respectively. For clusters without IMBHs, we ran simulations at three different metallicities given by [Fe/H] = −1.8, −1.3 and −0.7, respectively. For the later comparison with observed clusters, we always use those clusters from our grid that are closest in metallicity to the metallicity of the observed clusters. This should be accurate enough since metallicity-dependent effects on the internal cluster evolution are largely removed due to our scaling procedure described below so that the influence of cluster metallicity on our results (e.g. cluster mass) is small.

Simulations were run up to an age of $T = 13.5$ Gyr, and we stored data spaced by $T = 50$ Myr for all times between $T = 10.5$ and 13.5 Gyr. In order to compare our grid of simulations to the observed clusters, we combined 10 snapshots spanning a $T = 500$ Myr time span centred around the age of each cluster. Since we ran three different realizations for each grid point, our final models after combining the individual snapshots contained roughly 3×10^6 stars per grid point, which is larger than the actual number of stars in most observed clusters.

For [Fe/H] = −1.3, we also ran simulations with central IMBHs, choosing the IMBH masses such that the mass ratio of the IMBH to the total cluster mass at the end of our simulations ($T = 13.5$ Gyr) was equal to $M_{\rm IMBH}/M_{\rm GC} = 0.005$, 0.01 and 0.02, respectively. The initial concentrations and half-mass radii of these models were varied in the same way as for the no-IMBH models described above. All clusters in this paper were isolated, however we plan to add external tidal fields in subsequent papers when we compare the internal mass function of stars at different radii with observations.

Since our simulations contain fewer stars than the actual GCs and have different half-mass radii at the end of the simulations, we need to scale our simulations to match the masses and sizes of the observed GCs. Our scaling procedure is the same as that used by Baumgardt et al. (2003b) who fitted the massive GC G1 in M31 by a set of *N*-body simulations, and Jalali et al. (2012) who fitted ω Cen by a set of *N*-body models. The basic assumption of the scaling is that since the simulated star clusters are isolated, they evolve only due to stellar evolution and two-body relaxation. Hence the simulations can be scaled to star clusters of different masses or radii as long as the scaling is done in such a way that the overall relaxation time remains constant. Using the definition of the half-mass relaxation time given by Spitzer (1987), this implies

$$\frac{r_{\rm NB}}{r_{\rm GC}} = \left(\frac{M_{\rm GC}}{M_{\rm NB}}\right)^{1/3} \left(\frac{ln\gamma\, N_{\rm NB}}{ln\gamma\, N_{\rm GC}}\right)^{2/3}, \quad (1)$$

where M is the mass of a cluster, r is its half-mass radius, $N = M/ < m >$ is the number of cluster stars, and the subscripts NB and GC refer, respectively, to a star cluster from our grid of *N*-body simulations and an observed GC that we want to model. γ is a constant in the Coulomb logarithm which we assume to be equal to 0.11 (Giersz & Heggie 1994).

We determine the projected half-light radius of a GC by integrating the observed surface density profile up to the outermost radius

for which data are available. For each simulated cluster, we then determine iteratively the scaling factor $f_r = r_{NB}/r_{GC}$ that is necessary so that the cluster from the *N*-body simulation has the same projected half-light radius inside the same limiting radius as the observed GC if put at the same distance as the observed GC. For the calculation of the surface brightness profiles of the simulated clusters, we converted the bolometric luminosities of NBODY6 to *V*-band luminosities using the conversion formulae given by Eggleton, Fitchett & Tout (1989). After determining the radial scaling factor f_r, we determine the corresponding mass scaling factor from equation (1) and then multiply the velocities of the stars in the *N*-body simulation by a factor

$$f_v = \left(\frac{r_{NB}}{r_{GC}}\right)^{1/2} \left(\frac{M_{GC}}{M_{NB}}\right)^{1/2}, \quad (2)$$

where the first term on the right-hand side is due to the change in radius and the second term is due to the change in cluster mass. After scaling the velocities, we calculate the surface density and line-of-sight and proper motion velocity dispersion profiles for the simulated clusters. In order to improve the statistical significance of our results in the cluster centres, we use the infinite projection method of Mashchenko & Sills (2005) when calculating surface density and velocity dispersion profiles. For the velocity dispersion profiles, we mimic the magnitude limits of the observations by using only stars brighter than the main-sequence turn-off to determine the line-of-sight velocity dispersion profile. To compare with the proper motion data of Watkins et al. (2015a), we use all stars brighter than 1 mag below the turn-off magnitude. The resulting velocity dispersion profiles differ due to mass segregation, however the differences are typically less than 5 per cent.

In order to increase the number of models that can be compared with each GC, we assume that the properties of the final cluster change linearly with the initial concentration c, the logarithm of the initial half-mass radius $\log r_h$ and the IMBH mass fraction M_{BH}/M_{GC} and interpolate between our grid points. In total, we use 300 interpolation values for each grid dimension and determine the best-fitting model to the observed surface brightness and velocity dispersion profile by means of a χ^2 test.

Fig. 1 shows the location of the best-fitting no-IMBH model for each GC within the simulated grid of models. In this figure, a small initial half-mass radius r_h implies a small initial relaxation time and therefore a more dynamically advanced GC. It does not necessarily imply that a cluster actually started with a small half-mass radius, although the relaxation time and half-mass radius are correlated with each other. Most clusters can be fitted with clusters starting with half-mass radii around 5 pc, implying an initial relaxation time of $T_{RH} \approx 1$ Gyr. The best-fitting models of most GCs are located within our grid boundaries, however for nine GCs, we need models with the lowest modelled King concentration parameter of $c = 0.2$ to fit their surface density profiles. Figs B1–B13 show that we nevertheless usually obtain very good fits to their surface density and velocity dispersion profiles, so the low initial concentrations are not of immediate concern. They might however be an indication that either the surface density profiles of these clusters are influenced by the tidal field of the Milky Way or ongoing mass loss, processes which are not included in our simulations. Indeed most of these clusters have small galactocentric radii ($R_G < 5$ kpc) where tidal effects should be most important. Alternatively, a compact cluster of stellar mass black holes might prevent the cores of these clusters from collapsing (Morscher et al. 2013; Lützgendorf, Baumgardt & Kruijssen 2013). Indeed, this possibility has been suggested by Mackey et al. (2007) to explain the large core radii of young star clusters in the LMC and more recently by Peuten et al. (2016) to explain the absence of mass segregation in NGC 6101. Additional simulations will be necessary to distinguish between these possibilities.

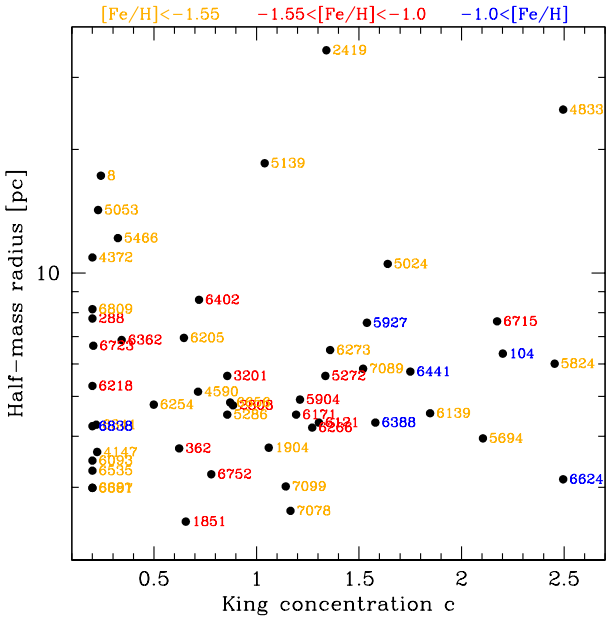

Figure 1. Location of the best-fitting no-IMBH model for each globular cluster (GC) within the simulated grid of models. Individual GCs are marked by their NGC numbers. Small half-mass radii imply small initial relaxation times and therefore dynamically more advanced GCs. Most GCs can be fitted by models starting from initial half-mass radii between 3 and 7 pc corresponding to initial relaxation times between 0.5 and 2 Gyr.

2.1 Validation

In order to test how well our fitting method can reproduce star cluster masses from their surface density and velocity dispersion profiles, we apply our models to the *N*-body simulations uf13 and uf14 from Lamers, Baumgardt & Gieles (2013) and models D1 and D2 from the DRAGON simulation (Wang et al. 2016a). We use four snapshots of simulations uf13 and uf14 between $T = 11.5$ and 12.5 Gyr and one snapshot of models D1 and D2 at $T = 12$ Gyr and calculate the surface density and velocity dispersion profile using all stars that are still bound to the clusters at these times. We then apply our fitting method to the four clusters. Fig. 2 compares the derived masses with the true masses of the simulated clusters (red circles). By the time the snapshots are created, the simulated clusters have lost 12 per cent to 75 per cent of their initial mass and for some of the clusters the mass function has already evolved significantly away from a Kroupa mass function. Nevertheless our fitting method reproduces the cluster masses to within 10 per cent. It performs slightly better for the dynamically less evolved clusters of the DRAGON simulation and less well for the highly evolved clusters from Lamers et al. (2013).

As a second check, we compare the results of our fitting method with the results of the Monte Carlo simulations aimed to reproduce the luminosity and velocity dispersion profiles and the luminosity function of stars in a number of GCs. The Monte Carlo results were published by Giersz & Heggie (2011) (for NGC 104), Heggie & Giersz (2008) (NGC 6121), Giersz & Heggie (2009) (NGC6397) and Heggie & Giersz (2014) (NGC 6656). For all clusters, we adopt

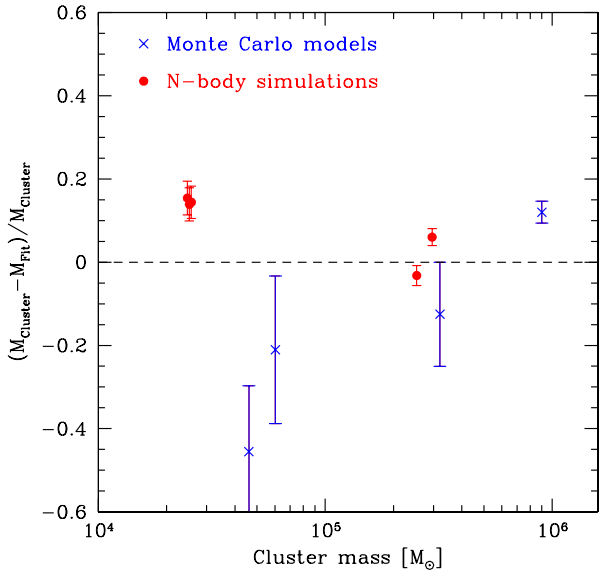

Figure 2. Comparison of the masses derived from our grid of *N*-body simulations with the true masses of star clusters in *N*-body simulations (red circles) and the masses of Galactic globular clusters (GCs) derived by fitting the results of Monte Carlo simulations (blue crosses). Our mass estimates reproduce the true masses of star clusters in *N*-body simulations to within 10 per cent and are within 20 per cent of the masses of Galactic GCs derived from Monte Carlo simulations.

the same distances as assumed by Giersz & Heggie and use only the velocity dispersion data which Giersz & Heggie used for each cluster. Fig. 2 compares the masses which we derive from *N*-body models with those found in the Monte Carlo simulations. We can reproduce the masses from the Monte Carlo simulations to within ∼20 per cent. The deviations are again larger for the dynamically more evolved clusters NGC 6121 and NGC 6397 and better for the more massive clusters NGC 104 and NGC 6656. The reason for the larger deviation of the Monte Carlo models compared to the *N*-body simulations is probably the small number of radial velocity data points of the observed clusters, which leave large freedom in the mass profiles and total cluster masses. We conclude that our models can reproduce cluster masses to within 10 per cent for clusters that have a well-determined radial velocity dispersion profile. Better mass estimates will probably require knowledge of the internal mass function of the cluster stars in addition to the clusters' velocity dispersion and surface density profile.

3 GLOBULAR CLUSTER DATA

We first determined the radial velocity dispersion profiles of Galactic GCs from individual radial velocity measurements of their member stars published in the literature. To this end, we searched the astronomical literature for published radial velocity measurements, excluding small data sets with less than ≈20 stars. In total, we found 95 publications containing about 25 500 individual radial velocities of stars in 45 clusters. About one third of the radial velocity measurements were from the three, recent large-scale surveys of Lane et al. (2011), Lardo et al. (2015) and Kimmig et al. (2015), of which each contains radial velocity information for several thousand stars. The rest of the data come from smaller data sets. For nine GCs, we also included radial velocities from the APOGEE survey (Majewski et al. 2016), which has measured abundances and radial velocities for over 150 000 red giants, including several hundred stars in GCs. Information on the papers used as input for calculating the radial velocity dispersion profiles can be found in Table A1.[1]

For each individual set of radial velocities, we first calculated the average cluster velocity using the method of Pryor & Meylan (1993) and using all stars which roughly fall within the radial velocity range of the cluster. We then subtracted the average cluster velocity from the individual measurements and merged all radial velocity data sets into a master catalogue for each cluster, containing the positions, radial velocities and radial velocity errors of all stars. We then use the stellar positions to identify stars with multiple measurements and calculate a weighted mean radial velocity and the corresponding error for each star with multiple measurements. Stars for which the individual radial velocity measurements show too strong a deviation from the mean were rejected as binaries. After removing binary stars, we put the stars into radial bins and calculated the radial velocity dispersion $\sigma_{\rm bin}$ by determining the maximum of the likelihood function

$$\log L = -\frac{1}{2}\sum_{i=1}^{N} \ln\left(\sigma_{\rm bin}^2 + e_i^2\right) + \sum_{i=1}^{N} \frac{v_i^2}{\sigma_{\rm bin}^2 + e_i^2} \quad (3)$$

based on all stars in a bin. Here v_i and e_i are the radial velocity and its respective error of each individual star. The standard deviation of the velocity dispersion was calculated by determining the velocity dispersion where the likelihood is less than 0.5 the maximum value in each direction. After the velocity dispersion of a radial bin was determined, we calculated the deviation of each star from the cluster mean according to

$$\chi^2 = \frac{v_i^2}{\sigma^2 + e_i^2} \quad (4)$$

and rejected all stars as binaries or background stars that deviated more than three standard deviations from the mean. We repeated the above procedure for each bin until we found a stable value for the velocity dispersion and the list of member stars. Depending on the number of radial velocity measurements available for a cluster, we used between 20 and 250 stars per bin to calculate the radial velocity dispersion. In order to calculate the radial velocity dispersion profile, we used the positions determined by Goldsbury, Heyl & Richer (2013) as cluster centres, except for NGC 1904, NGC 5694, NGC 5824 and NGC 6266 where we used the centres determined by Lützgendorf et al. (2013). This was necessary in order to get a radial velocity dispersion profile centred on the same position as the integral-field unit (IFU) data published by Lützgendorf et al. (2013). For clusters that contain a significant number of stars at large distances from the cluster centre, we used proper motions from the PPMXL catalogue (Roeser, Demleitner & Schilbach 2010) to help separate cluster members from non-members. PPMXL data were only used to separate members from non-members for stars more than a few hundred arcsec away from the cluster centre since for stars closer to the centre PPMXL proper motions were either not available or were found to be unreliable, presumably due to the strong crowding of stars towards the cluster centres.

In addition to the radial velocity dispersion data, we also used velocity dispersion data based on individual stellar proper motions to constrain the cluster kinematics. Most of the proper motion dispersion profiles were taken from Watkins et al. (2015a), who published velocity dispersion profiles for 21 clusters. We excluded NGC 7099 since the proper motion dispersion profile from Watkins et al.

[1] The radial velocity dispersion profiles can be downloaded from https://people.smp.uq.edu.au/HolgerBaumgardt/globular/.

(2015a) disagrees significantly with the radial velocity dispersion profile calculated in this paper for any reasonable cluster distance. As discussed by Watkins et al. (2015a), this might be due to the small number of stars which have measured proper motions in this cluster. We finally used velocity dispersion measurements based on IFU spectroscopy. IFU spectroscopy was available for nine clusters (NGC 1851, 1904, 2808, 5286, 5694, 5824, 6093, 6266and NGC 6388).

The surface brightness profiles were taken mainly from Trager, King & Djorgovski (1995). If available for a cluster, we replaced the Trager et al. profile in the cluster centre with an *HST* surface brightness profiles published by Noyola & Gebhardt (2006). For a few clusters, we took the surface density profiles from other literature sources. These cases are listed in Table A1 in the Appendix. For NGC 5927, the surface density profile calculated by Trager et al. (1995) has a bump in the centre that is impossible to reproduce by our modelling. Since no other cluster shows such a feature, the surface density profile might be influenced by a few bright stars in the centre. We therefore calculated a surface brightness profile based on the number counts of bright stars published by the ACS Survey of Galactic GCs (Sarajedini et al. 2007). The same was done for NGC 4833 where we combined the data published by Melbourne et al. (2000) with the ACS data to calculate the surface density profile.

16 clusters from our list have accurate proper motion dispersion profiles and also accurate enough radial velocity dispersion profiles so that their distances can be determined by χ^2 minimization of a simultaneous fit of our models to both profiles. From the fits, we are able to measure their distances to an accuracy of 50–450 pc and the distances are given in Table 2. For the remaining clusters, the distances were taken mainly from Ferraro et al. (1999), who determined GC distance moduli by CMD fitting. For clusters not studied by Ferraro et al. (1999), we took the distances from recent literature values. The adopted distances are listed in Table 1 together with the cluster ages and the calculated *V*-band magnitudes. The apparent *V*-band magnitudes and errors are calculated by taking the average of the apparent magnitudes given in Harris (1996), McLaughlin & van der Marel (2005), Dalessandro et al. (2012) and the integrated magnitudes determined in this work from the fit of our models to the surface brightness profiles. Cluster ages were taken from VandenBerg et al. (2013), or, if not available, from literature data. We finally took the cluster metallicities from the recent compilation by Carretta et al. (2009a) and the cluster reddenings from Harris (1996).

Table 1. Input parameters for the studied globular clusters. The sources for the distances are: F99: Ferraro et al. (1999), V07: Valenti, Ferraro & Origlia (2007), D11: Di Criscienzo et al. (2011), Z98: Zinn & Barnes (1998), H96: Harris (1996, 2010edition), tw: this work.

Name	Alt. Name	V (mag)	ΔV (mag)	Age (Gyr)	Dist. (kpc)	Dist. Source
NGC 104	47 Tuc	4.07	0.11	11.75	3.95	tw
NGC 288	–	8.16	0.07	11.50	8.80	tw
NGC 362	–	6.55	0.16	10.75	8.85	tw
NGC 1851	–	7.24	0.09	11.00	10.40	tw
NGC 1904	M 79	7.99	0.19	11.70	13.27	F99
NGC 2419	–	10.48	0.15	12.75	87.50	D11
NGC 2808	–	6.33	0.09	11.00	9.50	tw
NGC 3201	–	6.88	0.20	11.50	4.90	F99
NGC 4147	–	10.38	0.11	12.25	18.20	F99
NGC 4372	–	7.23	0.01	12.00	6.30	F99
NGC 4590	M 68	8.15	0.22	12.00	10.59	F99
NGC 4833	–	6.91	0.20	12.50	6.76	F99
NGC 5024	M 53	7.71	0.10	12.25	17.90	H96
NGC 5053	–	7.71	0.10	12.25	17.20	F99
NGC 5139	ω Cen	3.53	0.11	12.00	5.00	tw
NGC 5272	M 3	6.40	0.16	11.75	10.06	F99
NGC 5286	–	7.20	0.12	12.50	11.70	H96
NGC 5466	–	9.46	0.30	12.50	16.90	F99
NGC 5694	–	10.02	0.14	12.75	37.33	F99
NGC 5824	–	8.83	0.19	13.00	31.80	F99
NGC 5904	M 5	5.83	0.16	11.50	6.40	tw
NGC 5927	–	7.74	0.39	10.75	8.00	tw
NGC 6093	M 80	7.35	0.13	11.40	9.73	F99
NGC 6121	M 4	5.63	0.09	11.50	2.14	F99
NGC 6139	–	8.95	0.13	12.00	10.40	Z98
NGC 6171	M 107	8.18	0.31	12.00	6.09	F99
NGC 6205	M 13	5.80	0.10	12.00	7.60	F99
NGC 6218	M 12	6.92	0.28	13.00	5.22	F99
NGC 6254	M 10	6.42	0.38	11.75	4.71	F99
NGC 6266	M 62	6.45	0.12	11.40	6.55	tw
NGC 6273	M 19	6.80	0.05	12.75	8.24	V07
NGC 6341	M 92	6.51	0.06	12.75	8.10	tw
NGC 6362	–	7.67	0.10	12.50	7.60	H96
NGC 6388	–	6.76	0.13	11.75	11.00	tw
NGC 6397	–	5.77	0.18	13.00	2.40	tw
NGC 6402	M 14	7.66	0.08	11.50	9.30	H96
NGC 6441	–	7.16	0.11	11.00	13.49	V07
NGC 6535	–	11.14	0.57	12.75	7.28	H96
NGC 6624	–	7.78	0.13	11.25	8.43	V07
NGC 6656	M 22	5.07	0.07	12.50	2.66	tw
NGC 6681	M 70	7.98	0.15	12.75	9.89	F99
NGC 6715	M 54	7.47	0.10	11.75	23.50	tw
NGC 6723	–	7.11	0.17	12.50	8.20	V07
NGC 6752	–	5.52	0.17	12.50	3.90	tw
NGC 6809	M 55	6.63	0.24	13.00	5.75	F99
NGC 6838	M 71	7.84	0.49	11.00	3.86	F99
NGC 7078	M 15	6.13	0.10	12.75	9.90	tw
NGC 7089	M 2	6.43	0.03	11.75	11.50	H96
NGC 7099	M 30	7.25	0.24	13.00	8.67	F99
Terzan 8	–	12.11	0.32	13.00	26.73	F99

4 RESULTS

Figs B1–B13 compare our best-fitting profiles with the observed velocity dispersion and surface density profiles of GCs. Except for ω Cen and NGC 6715, all profiles shown are the no-IMBH models. As can be seen we usually obtain very good fits to the observed profiles. The surface brightness profiles of our best-fitting clusters are generally within 20 per cent of the observed surface brightness, despite the fact that the observed surface brightness profiles vary by up to 6 orders of magnitude in some clusters. Only beyond several hundred arcsec, some clusters show larger differences in their surface density profiles. This could be due to the influence of the Galactic tidal field which was not taken into account in our simulations, but might also be a result of observational uncertainties since a few hundred arcsec from the cluster centre the surface density of many GCs is already significantly below the background density of stars, making the determination of the outer surface density profiles uncertain. The differences with the measured velocity dispersion profiles are also usually less than 1 km s^{-1} and for most clusters within the observational uncertainties. The only clusters which cannot be well modelled by the no-IMBH models are ω Cen and M54 (NGC 6715). For these clusters, the observed velocity dispersion profile is significantly above our predictions in the centre and below in the outer parts. This could be due to an unseen mass concentration in the centre and we will discuss these clusters in greater detail

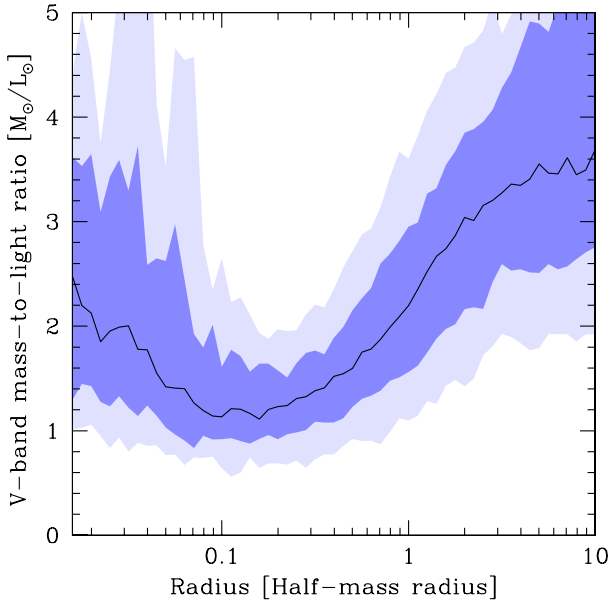

Figure 3. Local V-band mass-to-light ratios as a function of the distance to the cluster centre expressed in units of the half-mass radius. The average M/L ratio of all 50 clusters is shown by a solid line. Dark blue and light blue shaded regions mark the values of the M/L ratio which contain 68 per cent and 95 per cent of all clusters. The M/L ratio profiles of the clusters follow a U-shaped curve due to mass segregation, which concentrates high-mass compact remnants and giant stars in the cluster centre and pushes low-mass main-sequence stars towards the cluster outskirts.

in Section 4.1 when we will investigate the possible presence of IMBHs in GCs.

Fig. 3 depicts the V-band mass-to-light ratio profiles which we derive from our fits. The average mass-to-light ratio of all 50 clusters as a function of distance to the cluster centre is shown by a solid line and the regions in the M/L ratio that contain 68 per cent and 95 per cent of all clusters are shown by dark and light blue areas, respectively. In order to better compare individual clusters, we have divided the distances to the cluster centres by the half-mass radius of each cluster. It can be seen that the M/L ratios have a minimum between 0.1 and 0.2 half-mass radii. This minimum is due to the mass segregation of giant stars and high-mass main-sequence stars towards the cluster centre. Since giant stars dominate the cluster light but contain only a small fraction of the cluster mass, the M/L ratio decreases in the centre. Inside 0.1 half-mass radii the M/L ratios rise again since compact remnants like high-mass white dwarfs, neutron stars and black holes have masses even higher than the giant stars and are therefore more strongly concentrated towards the cluster centre. The M/L ratios also increase towards the outer cluster parts since low-mass main-sequence stars are pushed out of the cluster due to mass segregation. We also find that the importance of mass segregation depends on the relaxation time of a cluster. In clusters with very large relaxation times like NGC 2419, the M/L ratio changes by less than 30 per cent between the centre and the cluster halo. In contrast, for strongly mass-segregated clusters the variation of the M/L ratio can reach a factor of 4 between the core region and the cluster outskirts. This agrees with the recent results of Monte Carlo simulations by Bianchini et al. (2016), who found that the amount of mass segregation tightly correlates with the dynamical state of the cluster.

Table 2 presents a summary of our results. It gives the name of the cluster, the reduced χ^2 value from fitting the velocity dispersion and surface brightness profiles, the derived cluster mass and its error, the global M/L ratio and its error, and the best-fitting cluster distance and its error for those clusters where we derived cluster distances ourselves. Errors in the M/L ratio were calculated from the errors in cluster mass and cluster luminosity but do not include uncertainties in the cluster distances. The average V-band M/L_V ratio for our whole cluster sample is $M/L_V = 1.98 \pm 0.03$ $M_\odot/L_\odot$ and $M/L_V = 1.98 \pm 0.04$ $M_\odot/L_\odot$ if we restrict ourselves to clusters that have more than 200 radial velocity measurements and mass-to-light ratios with relative errors less than 30 per cent. If we split the more

Table 2. Derived parameters of the studied globular clusters.

Name	$\chi^2_{\rm red}$	Mass ($M_\odot$)	M/L Ratio	Distance (pc)
NGC 104	2.01	$7.00 \pm 0.06 \times 10^5$	1.99 ± 0.20	3950 ± 50
NGC 288	1.43	$8.76 \pm 0.26 \times 10^4$	2.23 ± 0.15	8800 ± 400
NGC 362	0.76	$3.21 \pm 0.06 \times 10^5$	1.73 ± 0.26	8850 ± 300
NGC 1851	1.81	$2.99 \pm 0.05 \times 10^5$	2.40 ± 0.20	10400 ± 200
NGC 1904	1.95	$2.20 \pm 0.18 \times 10^5$	2.23 ± 0.43	–
NGC 2419	2.60	$8.15 \pm 1.19 \times 10^5$	1.54 ± 0.22	–
NGC 2808	2.13	$8.29 \pm 0.06 \times 10^5$	1.96 ± 0.16	9500 ± 150
NGC 3201	1.51	$1.58 \pm 0.11 \times 10^5$	2.20 ± 0.43	–
NGC 4147	1.60	$5.32 \pm 1.71 \times 10^4$	2.45 ± 0.32	–
NGC 4372	0.32	$2.20 \pm 0.25 \times 10^5$	1.67 ± 0.19	–
NGC 4590	0.95	$8.45 \pm 1.71 \times 10^4$	1.39 ± 0.65	–
NGC 4833	0.74	$2.66 \pm 0.39 \times 10^5$	1.59 ± 0.33	–
NGC 5024	0.61	$3.83 \pm 0.51 \times 10^5$	1.60 ± 0.84	–
NGC 5053	0.54	$5.37 \pm 1.32 \times 10^4$	1.58 ± 0.54	–
NGC 5139	2.56	$2.95 \pm 0.02 \times 10^6$	2.54 ± 0.26	5000 ± 50
NGC 5272	1.85	$5.00 \pm 0.43 \times 10^5$	1.98 ± 0.37	–
NGC 5286	1.09	$4.61 \pm 0.23 \cdot \times 10^5$	1.51 ± 0.18	–
NGC 5466	0.92	$6.43 \pm 1.47 \times 10^4$	1.60 ± 0.56	–
NGC 5694	0.97	$4.22 \pm 0.45 \times 10^5$	2.79 ± 0.42	–
NGC 5824	0.32	$8.28 \pm 0.55 \times 10^5$	2.25 ± 0.42	–
NGC 5904	1.08	$3.08 \pm 0.04 \times 10^5$	1.74 ± 0.26	6400 ± 200
NGC 5927	1.96	$3.45 \pm 0.03 \times 10^5$	2.19 ± 0.42	8000 ± 400
NGC 6093	1.46	$3.37 \pm 0.16 \times 10^5$	2.18 ± 0.28	–
NGC 6121	0.89	$1.01 \pm 0.03 \times 10^5$	1.70 ± 0.15	–
NGC 6139	0.55	$5.31 \pm 1.22 \times 10^5$	2.59 ± 0.61	–
NGC 6171	0.96	$9.62 \pm 1.04 \times 10^4$	2.22 ± 0.69	–
NGC 6205	2.03	$5.00 \pm 0.42 \times 10^5$	2.06 ± 0.33	–
NGC 6218	0.70	$1.03 \pm 0.12 \times 10^5$	1.51 ± 0.40	–
NGC 6254	1.05	$2.26 \pm 0.29 \times 10^5$	1.99 ± 0.72	–
NGC 6266	1.58	$9.31 \pm 0.09 \times 10^5$	2.54 ± 0.28	6550 ± 140
NGC 6273	0.08	$9.21 \pm 1.62 \times 10^5$	2.83 ± 0.45	–
NGC 6341	0.74	$3.05 \pm 0.04 \times 10^5$	2.06 ± 0.12	8100 ± 150
NGC 6362	1.26	$1.44 \pm 0.05 \times 10^5$	2.64 ± 0.26	–
NGC 6388	1.11	$1.24 \pm 0.01 \times 10^6$	2.11 ± 0.26	11000 ± 450
NGC 6397	1.09	$9.40 \pm 0.32 \times 10^4$	2.33 ± 0.39	2400 ± 60
NGC 6402	1.43	$7.63 \pm 1.19 \times 10^5$	2.17 ± 0.37	–
NGC 6441	1.55	$1.86 \pm 0.02 \times 10^6$	2.30 ± 0.24	–
NGC 6535	2.28	$5.96 \pm 0.59 \times 10^4$	14.29 ± 7.93	–
NGC 6624	1.70	$2.42 \pm 0.07 \times 10^5$	2.33 ± 0.29	–
NGC 6656	0.93	$3.21 \pm 0.04 \times 10^5$	2.15 ± 0.14	2660 ± 100
NGC 6681	1.31	$1.72 \pm 0.04 \times 10^5$	2.62 ± 0.36	–
NGC 6715	5.07	$1.62 \pm 0.03 \times 10^6$	2.18 ± 0.20	23500 ± 300
NGC 6723	0.26	$1.96 \pm 0.40 \times 10^5$	2.06 ± 0.41	–
NGC 6752	0.71	$2.34 \pm 0.04 \times 10^5$	2.60 ± 0.41	3900 ± 100
NGC 6809	3.34	$1.78 \pm 0.15 \times 10^5$	2.25 ± 0.52	–
NGC 6838	1.43	$4.60 \pm 0.61 \times 10^4$	2.43 ± 1.18	–
NGC 7078	1.72	$5.01 \pm 0.06 \times 10^5$	1.27 ± 0.12	9900 ± 200
NGC 7089	0.46	$7.64 \pm 0.51 \times 10^5$	2.13 ± 0.15	–
NGC 7099	0.58	$1.21 \pm 0.10 \times 10^5$	1.37 ± 0.32	–
Terzan 8	0.49	$5.37 \pm 2.34 \times 10^4$	4.36 ± 2.96	–

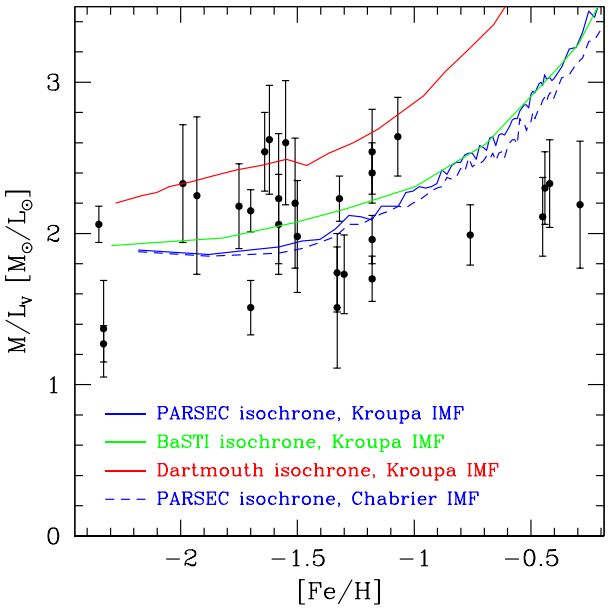

Figure 4. *V*-band mass-to-light ratios derived in this work as a function of metallicity. Solid lines show the predicted mass-to-light ratios for a Kroupa IMF according to the PARSEC (blue), BaSTI (green), and Dartmouth (red) isochrones for an age of $T = 12.5$ Gyr. The dashed blue line shows the predicted M/L ratio from the PARSEC isochrones for a Chabrier IMF. Except for the Dartmouth isochrones, our derived M/L ratios agree well with the theoretical predictions for either a Kroupa or Chabrier IMF.

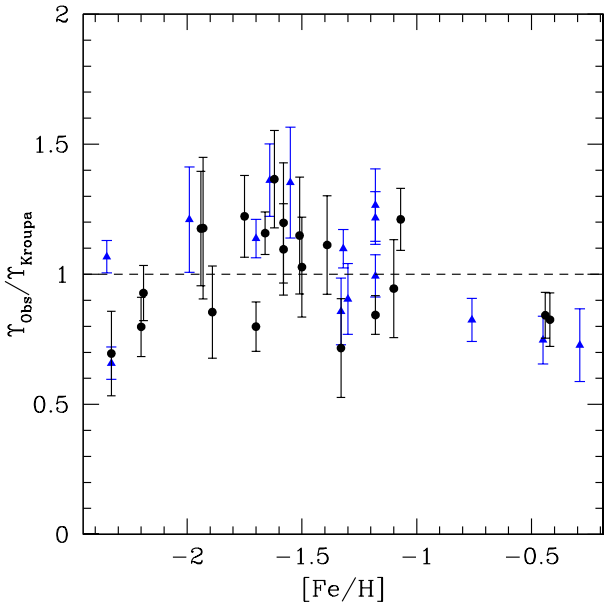

Figure 5. Ratio of the measured M/L ratios to the M/L ratios predicted by the PARSEC isochrones for clusters with a Kroupa IMF at the measured ages of the clusters as a function of cluster metallicity. Blue triangles mark clusters for which the distances were determined in this work. The average $\Upsilon_{\rm Obs}/\Upsilon_{\rm Kroupa}$ ratio is close to unity, indicating that most clusters have mass functions compatible with a Kroupa IMF.

accurate cluster sample into two sub-samples depending on cluster metallicity, we derive a mean *V*-band mass-to-light ratio of $M/L_V = 1.88 \pm 0.06$ M$_\odot$/L$_\odot$ for the metal-poor clusters with [Fe/H]<-1.5 and $M/L_V = 2.07 \pm 0.06$ M$_\odot$/L$_\odot$ for the metal-rich clusters. This increase of the average mass-to-light ratio with metallicity is in general agreement with the predictions from the stellar evolution theory.

Fig. 4 compares the global M/L ratios derived here with the predictions of stellar evolution models. Shown are predicted M/L ratios from PARSEC (Bressan et al. 2012), α-enhanced BaSTI (Pietrinferni et al. 2006) and α-enhanced Dartmouth isochrones (Dotter et al. 2008). The theoretical M/L_V values were calculated assuming a Kroupa (2001) initial mass function (IMF) with mass limits of 0.1 and 100 M$_\odot$, the Kalirai et al. (2008) initial-final mass ratio for white dwarfs and a 10 per cent retention fraction of neutron stars and black holes in the clusters. For the PARSEC isochrones, we also calculated M/L_V ratios for stars distributed according to a Chabrier (2003) IMF between the mass limits of 0.1 and 100 M$_\odot$. Since the BaSTI isochrones only give luminosities for stars with masses larger than 0.5 M$_\odot$, we used PARSEC luminosities for less massive stars. For clarity, we show only clusters with more than 200 radial velocity measurements and mass-to-light ratios with relative errors less than 30 per cent in Fig. 4, however the full cluster sample has a very similar distribution. It can be seen that the derived mass-to-light ratios are in general agreement with the PARSEC and BaSTI isochrones, especially at low metallicity. The agreement is less good for the Dartmouth isochrones, however these isochrones have a less detailed treatment of giant star evolution than either the BaSTI or PARSEC isochrones. Since giant stars dominate the cluster light, we regard the predictions of the BaSTI or PARSEC isochrones as more reliable.

Strader et al. (2011) found a decrease of the M/L ratio down to about $M/L_V \approx 1$ M$_\odot$/L$_\odot$ for solar metallicity for GCs in M31, which they attributed to a systematic change of the IMF with metallicity. We do not see a decrease in the M/L ratio with increasing metallicity. A possible reason could be that Strader et al. (2011) fitted single-mass King models to derive the global velocity dispersion from the measured central one. This would have produced a bias in the derived masses if clusters were mass segregated.

In order to better compare the derived M/L ratios with the predictions of stellar evolution models, we depict in Fig. 5 the ratio of the observed M/L ratio $\Upsilon_{\rm Obs} = M/L_V$ to $\Upsilon_{\rm Kroupa}$, the M/L_V ratio predicted by the PARSEC isochrones for clusters with a Kroupa IMF at the measured age of each individual cluster. The average $\Upsilon_{\rm Obs}/\Upsilon_{\rm Kroupa}$ ratio for all clusters shown in Fig. 5 is $<\Upsilon_{\rm Obs}/\Upsilon_{\rm Kroupa}> = 0.97 \pm 0.03$, compatible with unity. In particular the metal-poor clusters have M/L ratios in good agreement with a Kroupa IMF. Kruijssen & Mieske (2009) and Kimmig et al. (2015) found that the dynamical mass-to-light M/L ratios of GCs are systematically lower than those expected from canonical stellar population models. This was interpreted by Kruijssen & Mieske (2009) as due to ongoing cluster dissolution. We cannot confirm their results for the majority of GCs. The only clusters which are systematically below unity are the metal-rich clusters with [Fe/H]>-1. This could indicate a different present-day mass function, possible due to either a different IMF or the ongoing dissolution. However we have only five clusters with [Fe/H]>-1 in our sample and their $\Upsilon_{\rm Obs}/\Upsilon_{\rm Kroupa}$ ratios are within the range of values seen for the low-metallicity clusters. It therefore remains an open question if the mass function of the high-metallicity clusters is really different from that of the low-metallicity ones and, if true, where this difference is coming from.

4.1 Intermediate-mass black holes

IMBHs are black holes in the mass range of10^2–10^5 M$_\odot$. They might provide the missing link between stellar mass black holes

formed as the end product of stellar evolution and the supermassive black holes found in the centres of galaxies. In the last few years, evidence for the existence of IMBHs has been accumulating. Barth et al. (2004) for example found a 10^5 $M_\odot$ black hole at the centre of the Seyfert 1 galaxy POX 52 based on the broadness of the Hβ profile. Farrell et al. (2009) found evidence that the ultra-luminous X-ray source in the galaxy ESO243-49 is powered by an accreting black hole with a mass between 10^2 and 10^5 $M_\odot$. The IMBH nature of the accreting black hole was later confirmed by Webb et al. (2010) and Servillat et al. (2011).

Evidence for the existence of IMBHs in GCs is more controversial mainly due to the fact that a centrally concentrated cluster of compact remnants can produce a rise in the velocity dispersion profile similar to an IMBH. Gerssen et al. (2002) found evidence for the existence of a 4000 $M_\odot$ IMBH in the Galactic GC M15 based on radial velocity measurements of individual stars near the cluster centre. However, Baumgardt et al. (2003a) performed *N*-body simulations of star clusters without IMBHs and found that they could reproduce the radial velocity and surface density profile of M15 without the need for a central IMBH. Noyola et al. (2010) and Jalali et al. (2012) reported evidence for a 50000 $M_\odot$ IMBH in the GC ω Cen based on the VLT-FLAMES integrated spectra of the central parts of the cluster and detailed *N*-body models. In contrast, van der Marel & Anderson (2010) found that the velocity dispersion increase in the centre can be explained by a radially anisotropic velocity dispersion profile and derived a 1σ upper limit of only 12000 $M_\odot$ for any possible IMBH.

Lützgendorf et al. (2011) presented results from ground-based VLT/FLAMES spectroscopy in combination with an *HST* data for the GC NGC 6388 and found a very large central velocity dispersion of 25 km s^{-1} in this cluster, which they could only explain by an IMBH with a mass of $1.7 \pm 0.9 \times 10^4$ $M_\odot$. Lanzoni et al. (2013) and Lapenna et al. (2015) on the other hand obtained VLT FLAMES and KMOS spectra of 52 and 82 giant stars near the cluster centre and found a low central velocity dispersion of about 13 km s^{-1}, which limited the mass of any central black hole to less than 2000 $M_\odot$. In a re-analysis of all existing data, Lützgendorf et al. (2015) found that individual radial velocities in the core of NGC 6388 are systematically biased towards the mean cluster velocity due to the blending of stars as a result of the high central density. By simulating this effect using artificially created IFU data cubes, they confirmed their initial high value for the velocity dispersion and derived an IMBH mass of $2.8 \pm 0.4 \times 10^4$ $M_\odot$. IMBH detections were furthermore reported by Lützgendorf et al. (2013) for NGC 1904 ($M_{\rm BH} = 3000 \pm 1000$ $M_\odot$) and NGC 6266 ($M_{\rm BH} = 2000 \pm 1000$ $M_\odot$), Feldmeier et al. (2013) for NGC 5286 ($M_{\rm BH} = 1500 \pm 1000$ $M_\odot$), Ibata et al. (2009) for NGC 6715 ($M_{\rm BH} \approx 9400$ $M_\odot$) and most recently by Kamann et al. (2016) for NGC 6397 ($M_{\rm BH} \approx 600$ $M_\odot$).

Figs 6 and 7 depict the surface density profiles of the above-mentioned eight clusters and compare the observed profiles with the best-fitting no-IMBH models and the best-fitting IMBH models from our grid of *N*-body simulations. The best-fitting IMBH models were obtained by interpolating only among models with IMBHs. Since we calculated models containing IMBHs with masses of 0.5 per cent, 1 per cent and 2 per cent of the final cluster mass, the IMBH models are restricted to IMBH mass fractions between 0.5 per cent and 2 per cent of the cluster mass.

In NGC 1904, the best-fitting IMBH model does significantly worse than the best-fitting no-IMBH model; the reduced χ^2 value for the IMBH model is 2.36 as opposed to 1.12 for the best-fitting IMBH model. The reason is the poor fit of the observed surface density profile in the innermost 30 arcsec; for the velocity dispersion data alone, both IMBH and no-IMBH model do about equally well. The reason for the bad fit of the surface density profile is the fact that star clusters with IMBHs have a weak cusp in surface density as a result of mass segregation and energy equipartition (Baumgardt, Makino & Hut 2005). This, together with the fact that NGC 1904 has a relatively small relaxation time ($T \approx 3$ Gyr), means that no IMBH model is able to reproduce the observed surface density profile after a Hubble time, independent of the starting density profile. We conclude that NGC 1904 does not contain an IMBH. A similar problem exists for NGC 6266 (lowest panels of Fig. 6). The problem is even more apparent for NGC 6397 and NGC 7078 (M15), both clusters with very steeply rising central density profiles which are in complete disagreement with how IMBH models at the same dynamical age look like (see Fig. 7).

In NGC 5286, the IMBH model fits the observed profiles marginally better than the best-fitting no-IMBH model. However, since the best-fitting no-IMBH model has a reduced χ^2 value near one, the IMBH detection is not significant. This confirms the results of Feldmeier et al. (2013). In NGC 6388, the best-fitting no-IMBH model fits the surface density profile better than the best-fitting IMBH model. Unfortunately the velocity dispersion profile in the central few arcsec is highly controversial in this cluster. If the central velocity dispersion is as low as 13 km s^{-1} as found by Lanzoni et al. (2013), the cluster definitely does not contain an IMBH, while if the velocity dispersion profile is rising as found by Lützgendorf et al. (2015), an IMBH could be present. Interestingly, we have difficulties reproducing both the low velocity dispersion from Lanzoni et al. (2013) with a no IMBH model and the high velocity dispersion found by Lützgendorf et al. (2015) with our best-fitting IMBH model, which could be an indication that both values are biased to too low/high values. A final decision on whether an IMBH is present in NGC 6388 or not can only be made once the velocity dispersion profile in the centre of the cluster is known.

The cluster with the strongest evidence for an IMBH is ω Cen. Our best-fitting no-IMBH model provides a very poor fit to the velocity dispersion profile. It has a reduced $\chi^2_{\rm r}$ value of 2.72, the second highest $\chi^2_{\rm r}$ value of all clusters in our sample after NGC 6715. An unsegregated, isotropic star cluster without an IMBH can therefore be safely excluded as the starting condition for ω Cen. In contrast, an IMBH model with an IMBH of 40 000 $M_\odot$ has a reduced χ^2 value of only 1.71. Fig. 6 shows that this model provides a much better fit than the no-IMBH model, the $\chi^2_{\rm r}$ value is larger than one mainly because the measured data points have very small error bars of only a few hundred m s^{-1}. Given the limited range of models which we can explore, it is difficult to reproduce any velocity dispersion profile to such a level of precision. Zocchi, Gieles & Hénault-Brunet (2016a) have argued that radially anisotropic velocity dispersion profiles could create a similar increase in the velocity dispersion profile as a central IMBH. In addition, van der Marel & Anderson (2010) found that anisotropic models provided a better fit to the velocity dispersion profile of ω Cen than isotropic models with central IMBHs. While the models of van der Marel & Anderson (2010) took mass segregation of stars into account, it is not clear how realistic their approach was. A look at their fig. 7, for example, shows that their isotropic no-IMBH model is already in very good agreement with the observed velocity dispersion profile, while it provides a very poor fit in our case. It is therefore not clear if the inclusion of radial anisotropy would change the velocity dispersion profile by a large enough amount to bring our models without IMBHs into agreement with the observations, especially since van der Marel & Anderson (2010) and the proper motion data

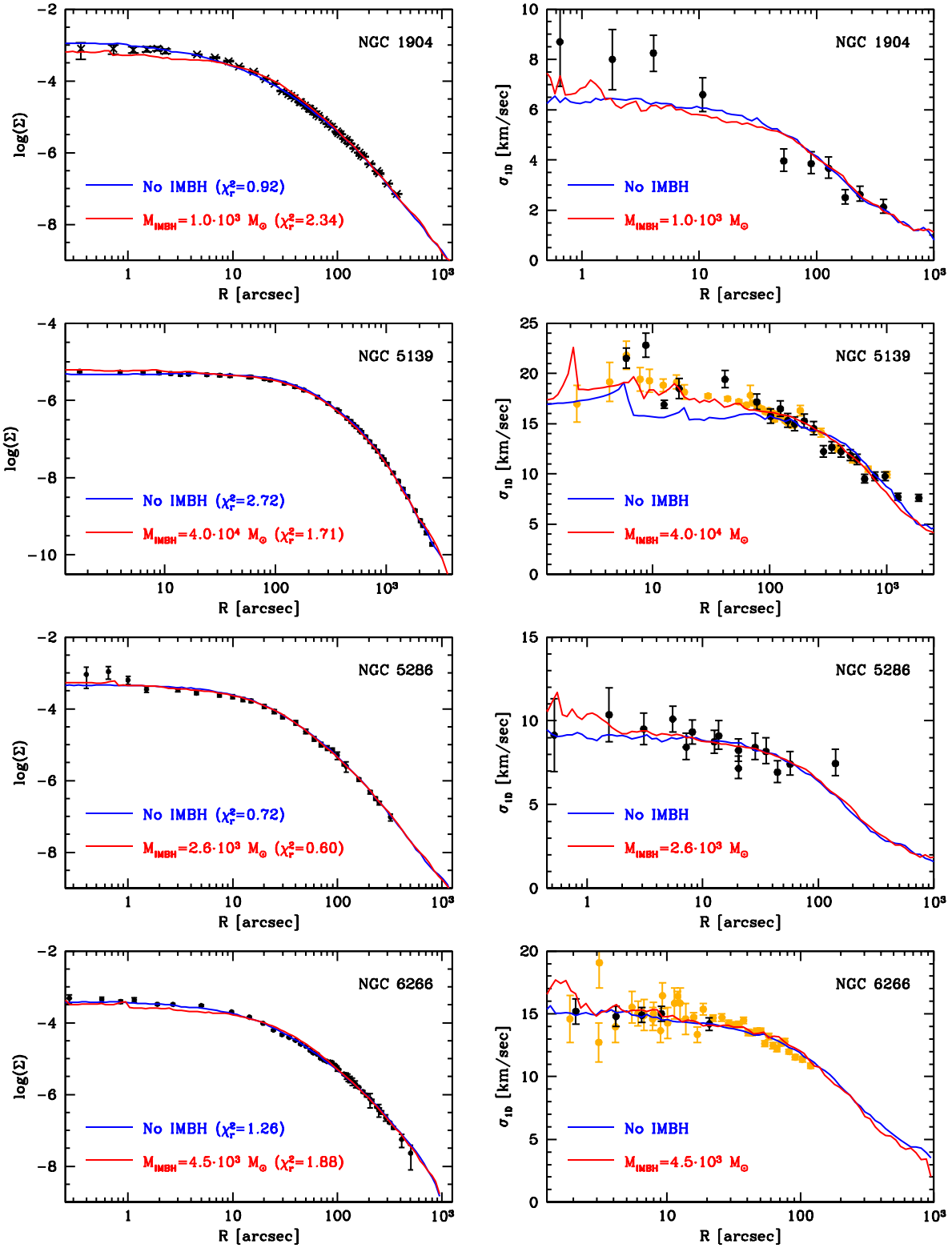

Figure 6. Fit of the surface density profiles (left-hand panels) and velocity dispersion profiles (right-hand panels) of the globular clusters NGC 1904, NGC 5139, NGC 5286 and NGC 6266 for which previous literature work found evidence for the presence of IMBHs. For each cluster we show the best-fitting *N*-body models with (red lines) and without (blue lines) IMBHs. The IMBH models were obtained by interpolating between the grid of models containing IMBHs between 0.5 per cent and 2 per cent of the total cluster mass. The best-fitting IMBH models fit the observed surface density profiles worse for NGC 1904 and NGC 6266 and do not improve the fits of the velocity dispersion profiles, indicating that the clusters do not contain IMBHs. For NGC 5286, both no-IMBH and IMBH models provide a good fit. In NGC 5139, a model with an IMBH of 4.1×10^4 $M_\odot$ provides a significantly better fit of the surface density and velocity dispersion profile than a no-IMBH model, making this cluster the cluster which shows the strongest evidence for an IMBH.

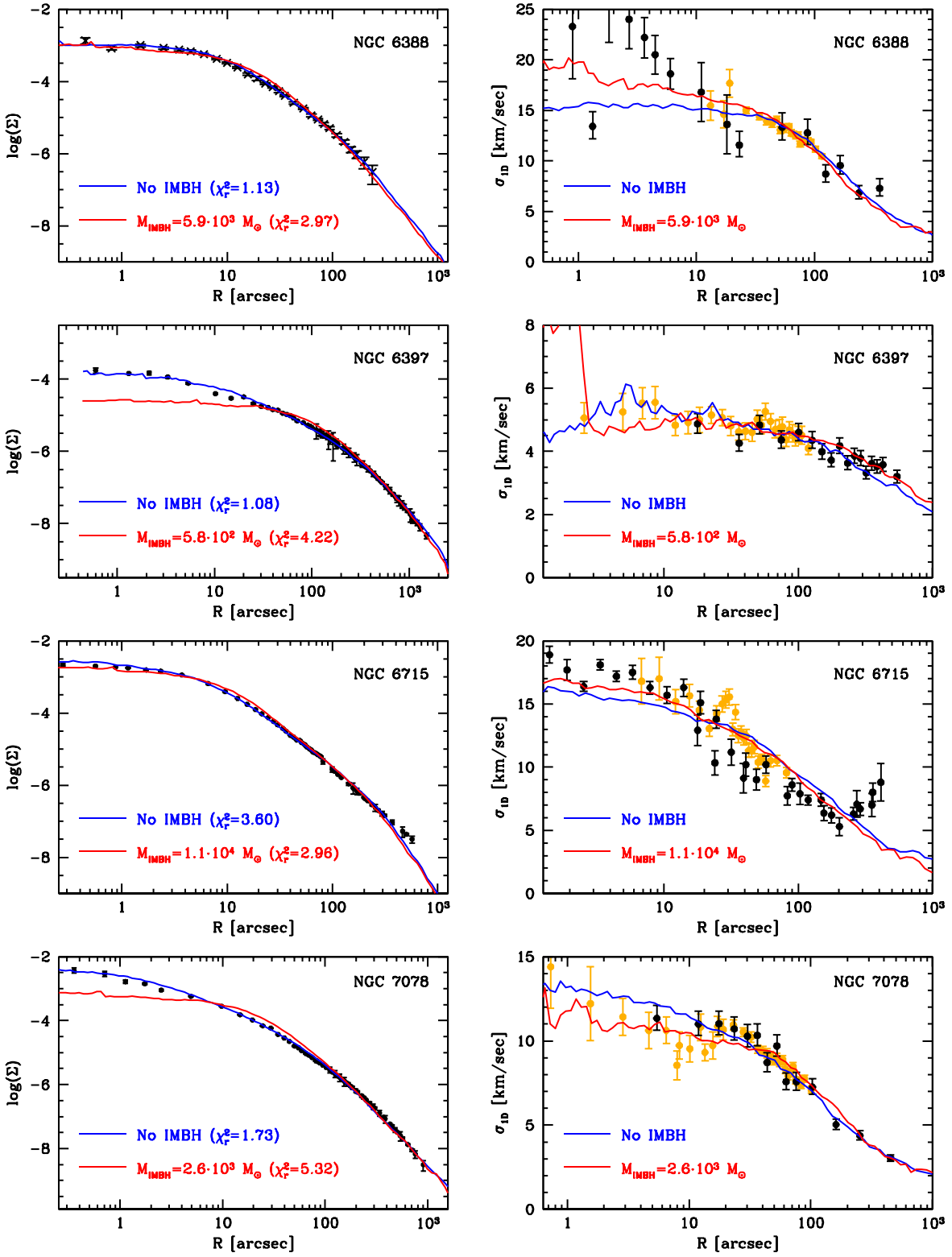

Figure 7. Same as Fig. 6 for the globular clusters NGC 6388, NGC 6397, NGC 6715 and NGC 7078. IMBHs are excluded for NGC 6397 and 7078 due to the very poor fit of the surface density profiles. In NGC 6388, IMBH models provide a less good fit to the surface density profile than the no IMBH model, however the uncertainty about the central velocity dispersion profile prevents us from drawing any firm conclusions. In NGC 6715, a model with a 11 000 $M_\odot$ IMBH provides a better fit to the velocity dispersion profile than a no IMBH model, but fits the surface density profile less well.

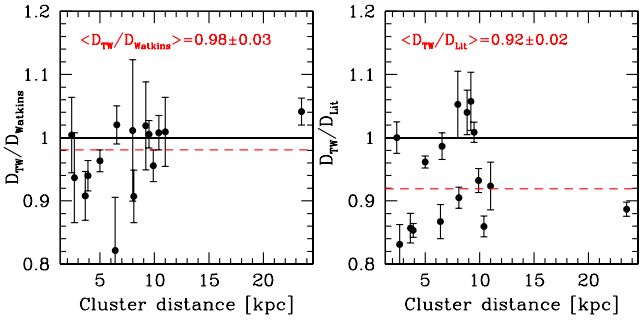

Figure 8. Ratio of the cluster distances derived in this work to the distances found by Watkins et al. (2015b) (left-hand panel) and cluster distances compiled from the literature (right-hand panel) for the clusters for which we have determined distances. Dashed lines show the average distance ratio in each panel. Our distances agree very well with the distances of Watkins et al. (2015b), but are on average about 8 per cent smaller than the literature distances.

of Watkins et al. show that ω Cen is essentially isotropic in its centre and only mildly radially anisotropic beyond 200 arcsec. It seems more likely that ω Cen contains either a dark cluster of compact remnants or a population of low-mass stars in its centre on the top of what mass segregation is already producing in our models, or a $\sim$40 000 $M_\odot$ IMBH. Comparison of the observed stellar mass function of stars at different radii will help to further refine our models and should hopefully clarify the situation.

In NGC 6715, a model with an IMBH of $M_{\rm IMBH} = 11\,000$ $M_\odot$ provides a slightly better fit to the velocity dispersion profile of the cluster but fits the central surface density profile less well. NGC 6715 (M54) has however the added complication that the cluster is the centre of the Sagittarius dwarf galaxy so that at each radius stars that are part of the nucleus of Sagittarius contribute to the surface density and velocity dispersion profile (Bellazzini et al. 2008). An increase in the fraction of Sagittarius stars is almost certainly responsible for the rise in the velocity dispersion profile seen beyond 200 arcsec. There is also still a significant discrepancy between the best-fitting IMBH model and the observed velocity dispersion profile of NGC 6715. Although an IMBH might be present in NGC 6715 as well, we regard the evidence for an IMBH in NGC 6715 as weaker than in ω Cen.

4.2 Cluster distances

Fig. 8 compares the cluster distances derived in this work with the distances derived by Watkins et al. (2015b) (left-hand panel) and cluster distances from the literature (right-hand panel). In order to derive the distances, we fitted our models to the surface density, radial velocity and proper motion dispersion profiles of the clusters and varied the distance until the combined χ^2 was minimal. Our distances are on average 2 per cent $\pm$ 3 per cent smaller than those of Watkins et al. (2015b) and hence in excellent agreement with their distances. The discrepancy is larger when we compare with literature distances, which are mainly obtained from CMD fitting since our distances are on average 8 per cent smaller. The literature distances were taken mostly from Ferraro et al. (1999), however we obtain a similar difference when using the Harris (1996) distances. We find no obvious correlation between the distance ratio $D_{\rm TW}/D_{\rm Lit}$ and any other cluster parameter like metallicity, total mass or cluster distance (see Fig. 8). It therefore remains unclear where the discrepancy between our distances and the literature values is coming from. Parallax data from the *GAIA* satellite should help to settle the GC distance scale.

4.3 Deviations from Newtonian dynamics?

Scarpa et al. (2007a) and Scarpa et al. (2011) reported evidence for a flattening of the velocity dispersion profile in the outermost parts of a number of GCs including NGC 288, NGC 1851, NGC 1904 and NGC 7099, which they attributed to a deviation from Newtonian dynamics. Our models give us a chance to verify their claims. As can be seen from Figs B1, B2 and B12, the measured velocity dispersion profiles of the four clusters studied by Scarpa et al. are compatible with predictions of our *N*-body models out to the outermost data points with no evidence for a breakdown of Newtonian mechanics. The same is the case for most other clusters. We attribute the difference to Scarpa et al. to the fact that we calculate velocity dispersion profiles based on a larger number of radial velocities, which allows us to more efficiently identify binaries and non-members. In addition, we apply a χ^2 test based on the local velocity dispersion to separate members from non-members, while Scarpa et al. include all stars as members that have radial velocities within certain velocity limits. In the outer parts of GCs, where a larger fraction of stars are non-members, the approach used by Scarpa et al. is likely to overestimate the velocity dispersion. The agreement with our models could probably be improved further since the simulations presented here do not include tidal fields, which increase the velocity dispersion of stars near the tidal radius (Küpper et al. 2010; Claydon, Gieles & Zocchi 2015).

The only cluster which deviates significantly from our predictions is NGC 6715 (M54), where the velocity dispersion profile rises in the outermost few 100 arcsec. As discussed by Bellazzini et al. (2008), this is most likely due to the fact that the sample includes stars from the Sagittarius dwarf galaxy, which follow a different kinematical profile and whose relative contribution increases in the outermost cluster parts. We have therefore neglected all data points beyond 200 arcsec in the dynamical analysis of this cluster. Apart from NGC 6715, the GC velocity dispersion profiles do not show any evidence for deviations from Newtonian dynamics out to distances of several 100 arcsec, corresponding to a physical distance of $\sim$10 pc.

5 CONCLUSIONS AND OUTLOOK

We have run a large grid of 900 *N*-body simulations of star clusters, varying the initial half-mass radius, density profile, cluster metallicity and the mass fraction of a central IMBH. We have also determined new radial velocity dispersion profiles of 50 Galactic GCs from about 25 000 published line-of-sight radial velocity measurements of stars in GCs, and combined these profiles with velocity dispersion data based on proper motions and published surface density profiles. By comparing the *N*-body data with the observed data and selecting the best-fitting model for each cluster, we were then able to derive absolute masses, mass-to-light ratios and limits on the possible presence of IMBH in the centres of all clusters. For a subset of 16 clusters for which both good proper motion and radial velocity information are available, we also determined the cluster distances.

We find that the average mass-to-light ratio of Galactic GCs is $<M/L_V> = 1.98 \pm 0.03$, which agrees very well with the expected M/L_V ratio for stars that formed with a standard Kroupa or Chabrier IMF. The mass-to-light ratios of high-metallicity clusters with [Fe/H]>-1 could be slightly lower than predicted by standard

stellar mass functions. The number of high-metallicity clusters in our sample is however small and the variation seen for them is within the variation found for low-metallicity clusters. Given the good agreement between the derived and the theoretically expected M/L ratios, there is no evidence that GC M/L ratios are significantly affected by ongoing cluster dissolution. More accurate M/L ratios, or M/L ratios for a wider range of cluster parameters will be necessary to determine what role dissolution has played for GCs.

We find strong evidence that ω Cen hosts an IMBH of $\sim$40 000 $M_\odot$ in its centre since the velocity dispersion profile of the cluster is in strong disagreement with *N*-body models without an IMBH. A compact cluster of stellar remnants in the centre or a cluster that starts with a radially anisotropic velocity dispersion profile might be alternatives to an IMBH, however these possibilities seem unlikely given how well our isotropic, non-mass-segregated models fit all other clusters. Given the absence of radio and X-ray emission from the centre of ω Cen (Maccarone, Fender & Tzioumis 2005; Haggard et al. 2013), this result implies that if an IMBH exists in the centre, it must accrete very little or with very low efficiency ($\eta < 10^{-9}$). Evidence for the presence of an IMBH is also found in NGC 6715 (M54), however in NGC 6715 the best-fitting IMBH model is still in significant disagreement with the velocity dispersion profile. We can strongly exclude the presence of IMBHs in NGC 6397 and M15 and find that they are also unlikely to be present in most other clusters since IMBH models provide significantly less good fits to the surface density profiles than no-IMBH models. We therefore conclude that if IMBHs exist in GCs, they can only exist in a small fraction of them.

In this work, we only compared the observed velocity dispersion and surface density profiles with the results from our *N*-body simulations. The next step is to also compare the mass function of stars at different radii with our predictions by performing simulations of star clusters which start with a range of IMFs and performing simulations that include cluster dissolution due to external tidal fields. Mass functions of stars have been observed for about half of all GCs from our sample by De Marchi, Paresce & Pulone (2007), Paust et al. (2010) and Sollima, Bellazzini & Lee (2012). Comparison of the stellar mass functions will allow to accurately predict the structural parameter of the clusters like core and half-mass radii and the corresponding densities and relaxation times. It will also allow to determine the starting conditions of GCs in terms of initial radii, IMFs and the amount of primordial mass segregation and thereby gain a much better understanding of their formation and evolution.

ACKNOWLEDGEMENTS

We thank Karl Gebhardt, Georges Meylan, Ben MacLean and Sandro Villanova for sharing unpublished radial velocity data with us. We are also grateful to Long Wang for sending us data from his simulations. We finally thank Pouria Khalaj and two anonymous referees for comments that helped improve the presentation of the paper. This work has made use of BaSTI web tools.

REFERENCES

Aarseth S. J., 1999, PASP, 111, 1333
Askar A., Szkudlarek M., Gondek-Rosińska D., Giersz M., Bulik T., 2017, MNRAS, 464, L36
Bailyn C. D., 1995, ARA&A, 33, 133
Banerjee S., Baumgardt H., Kroupa P., 2010, MNRAS, 402, 371
Barth A. J., Ho L. C., Rutledge R. E., Sargent W. L. W., 2004, ApJ, 607, 90
Battaglia G., Irwin M., Tolstoy E., Hill V., Helmi A., Letarte B., Jablonka P., 2008, MNRAS, 383, 183
Baumgardt H., Makino J., 2003, MNRAS, 340, 227
Baumgardt H., Hut P., Makino J., McMillan S., Portegies Zwart S., 2003a, ApJ, 582, L21
Baumgardt H., Makino J., Hut P., McMillan S., Portegies Zwart S., 2003b, ApJ, 589, L25
Baumgardt H., Makino J., Hut P., 2005, ApJ, 620, 238
Baumgardt H., Côté P., Hilker M., Rejkuba M., Mieske S., Djorgovski S. G., Stetson P., 2009, MNRAS, 396, 2051
Bellazzini M., 2007, A&A, 473, 171
Bellazzini M. et al., 2008, AJ, 136, 1147
Bellazzini M. et al., 2015, MNRAS, 446, 3130
Bianchini P., van de Ven G., Norris M. A., Schinnerer E., Varri A. L., 2016, MNRAS, 458, 3644
Boberg O. M., Friel E. D., Vesperini E., 2015, ApJ, 804, 109
Bragaglia A., Carretta E., Sollima A., Donati P., D'Orazi V., Gratton R. G., Lucatello S., Sneden C., 2015, A&A, 583, A69
Bressan A., Marigo P., Girardi L., Salasnich B., Dal Cero C., Rubele S., Nanni A., 2012, MNRAS, 427, 127
Cacciari C. et al., 2004, A&A, 413, 343
Carretta E., Bragaglia A., Gratton R. G., Leone F., Recio-Blanco A., Lucatello S., 2006, A&A, 450, 523
Carretta E. et al., 2007a, A&A, 464, 939
Carretta E., Bragaglia A., Gratton R. G., Lucatello S., Momany Y., 2007b, A&A, 464, 927
Carretta E., Bragaglia A., Gratton R., D'Orazi V., Lucatello S., 2009a, A&A, 508, 695
Carretta E. et al., 2009b, A&A, 505, 117
Carretta E. et al., 2010, A&A, 520, A95
Carretta E. et al., 2013, A&A, 557, A138
Carretta E. et al., 2014a, A&A, 564, A60
Carretta E., Bragaglia A., Gratton R. G., D'Orazi V., Lucatello S., Sollima A., 2014b, A&A, 561, A87
Carretta E. et al., 2015, A&A, 578, A116
Chabrier G., 2003, PASP, 115, 763
Claydon I., Gieles M., Zocchi A., 2015, IAU General Assembly, 22, 2253013
Cordero M. J., Pilachowski C. A., Johnson C. I., Vesperini E., 2015, ApJ, 800, 3
Cote P., Welch D. L., Fischer P., Gebhardt K., 1995, ApJ, 454, 788
Cote P., Pryor C., McClure R. D., Fletcher J. M., Hesser J. E., 1996, AJ, 112, 574
D'Orazi V. et al., 2015, MNRAS, 449, 4038
Da Costa G. S., 2012, ApJ, 751, 6
Da Costa G. S., 2016, MNRAS, 455, 199
Dalessandro E., Schiavon R. P., Rood R. T., Ferraro F. R., Sohn S. T., Lanzoni B., O'Connell R. W., 2012, AJ, 144, 126
Davies M. B., Piotto G., de Angeli F., 2004, MNRAS, 349, 129
De Marchi G., Paresce F., Pulone L., 2007, ApJ, 656, L65
Di Criscienzo M. et al., 2011, AJ, 141, 81
Dotter A., Chaboyer B., Jevremović D., Kostov V., Baron E., Ferguson J. W., 2008, ApJS, 178, 89
Downing J. M. B., Benacquista M. J., Giersz M., Spurzem R., 2011, MNRAS, 416, 133
Drukier G. A., Fahlman G. G., Richer H. B., 1992, ApJ, 386, 106
Drukier G. A., Slavin S. D., Cohn H. N., Lugger P. M., Berrington R. C., Murphy B. W., Seitzer P. O., 1998, AJ, 115, 708
Drukier G. A., Cohn H. N., Lugger P. M., Slavin S. D., Berrington R. C., Murphy B. W., 2007, AJ, 133, 1041
Eggleton P. P., Fitchett M. J., Tout C. A., 1989, ApJ, 347, 998
Farrell S. A., Webb N. A., Barret D., Godet O., Rodrigues J. M., 2009, Nature, 460, 73
Feldmeier A. et al., 2013, A&A, 554, A63
Ferraro F. R., Messineo M., Fusi Pecci F., de Palo M. A., Straniero O., Chieffi A., Limongi M., 1999, AJ, 118, 1738
Fischer P., Welch D. L., Mateo M., Cote P., 1993, AJ, 106, 1508
Gebhardt K., Pryor C., Williams T. B., Hesser J. E., 1995, AJ, 110, 1699

Gebhardt K., Pryor C., O'Connell R. D., Williams T. B., Hesser J. E., 2000, AJ, 119, 1268
Gerssen J., van der Marel R. P., Gebhardt K., Guhathakurta P., Peterson R. C., Pryor C., 2002, AJ, 124, 3270
Gieles M., Zocchi A., 2015, MNRAS, 454, 576
Giersz M., Heggie D. C., 1994, MNRAS, 268, 257
Giersz M., Heggie D. C., 2009, MNRAS, 395, 1173
Giersz M., Heggie D. C., 2011, MNRAS, 410, 2698
Giersz M., Leigh N., Hypki A., Lützgendorf N., Askar A., 2015, MNRAS, 454, 3150
Goldsbury R., Heyl J., Richer H., 2013, ApJ, 778, 57
Gratton R. G., Lucatello S., Carretta E., Bragaglia A., D'Orazi V., Momany Y. A., 2011, A&A, 534, A123
Gratton R. G. et al., 2012, A&A, 539, A19
Gratton R. G. et al., 2013, A&A, 549, A41
Gratton R. G. et al., 2014, A&A, 563, A13
Gratton R. G. et al., 2015, A&A, 573, A92
Gunn J. E., Griffin R. F., 1979, AJ, 84, 752
Haggard D., Cool A. M., Heinke C. O., van der Marel R., Cohn H. N., Lugger P. M., Anderson J., 2013, ApJ, 773, L31
Harris W. E., 1996, AJ, 112, 1487
Heggie D. C., Giersz M., 2008, MNRAS, 389, 1858
Heggie D. C., Giersz M., 2014, MNRAS, 439, 2459
Hilker M., Baumgardt H., Infante L., Drinkwater M., Evstigneeva E., Gregg M., 2007, A&A, 463, 119
Hurley J. R., Pols O. R., Tout C. A., 2000, MNRAS, 315, 543
Ibata R. et al., 2009, ApJ, 699, L169
Ibata R., Sollima A., Nipoti C., Bellazzini M., Chapman S. C., Dalessandro E., 2011, ApJ, 738, 186
Ivans I. I., Sneden C., Kraft R. P., Suntzeff N. B., Smith V. V., Langer G. E., Fulbright J. P., 1999, AJ, 118, 1273
Jalali B., Baumgardt H., Kissler-Patig M., Gebhardt K., Noyola E., Lützgendorf N., de Zeeuw P. T., 2012, A&A, 538, A19
Johnson C. I., Pilachowski C. A., Simmerer J., Schwenk D., 2008, ApJ, 681, 1505
Johnson C. I., Rich R. M., Pilachowski C. A., Caldwell N., Mateo M., Bailey J. I., III, Crane J. D., 2015, AJ, 150, 63
Kacharov N. et al., 2014, A&A, 567, A69
Kalirai J. S., Hansen B. M. S., Kelson D. D., Reitzel D. B., Rich R. M., Richer H. B., 2008, ApJ, 676, 594
Kamann S., Wisotzki L., Roth M. M., Gerssen J., Husser T.-O., Sandin C., Weilbacher P., 2014, A&A, 566, A58
Kamann S. et al., 2016, A&A, 588, A149
Kimmig B., Seth A., Ivans I. I., Strader J., Caldwell N., Anderton T., Gregersen D., 2015, AJ, 149, 53
King I., 1962, AJ, 67, 471
King I. R., 1966, AJ, 71, 64
Kravtsov A. V., Gnedin O. Y., 2005, ApJ, 623, 650
Kroupa P., 2001, MNRAS, 322, 231
Kruijssen J. M. D., Mieske S., 2009, A&A, 500, 785
Küpper A. H. W., Kroupa P., Baumgardt H., Heggie D. C., 2010, MNRAS, 407, 2241
Lamers H. J. G. L. M., Baumgardt H., Gieles M., 2013, MNRAS, 433, 1378
Lane R. R., Kiss L. L., Lewis G. F., Ibata R. A., Siebert A., Bedding T. R., Székely P., Szabó G. M., 2011, A&A, 530, A31
Lanzoni B. et al., 2013, ApJ, 769, 107
Lapenna E., Origlia L., Mucciarelli A., Lanzoni B., Ferraro F. R., Dalessandro E., Valenti E., Cirasuolo M., 2015, ApJ, 798, 23
Lardo C. et al., 2015, A&A, 573, A115
Lee Y. S. et al., 2008, AJ, 136, 2050
Lind K., Primas F., Charbonnel C., Grundahl F., Asplund M., 2009, A&A, 503, 545
Lovisi L., Mucciarelli A., Lanzoni B., Ferraro F. R., Gratton R., Dalessandro E., Contreras Ramos R., 2012, ApJ, 754, 91
Lovisi L., Mucciarelli A., Dalessandro E., Ferraro F. R., Lanzoni B., 2013, ApJ, 778, 64
Lucatello S., Sollima A., Gratton R., Vesperini E., D'Orazi V., Carretta E., Bragaglia A., 2015, A&A, 584, A52
Lupton R. H., Gunn J. E., Griffin R. F., 1987, AJ, 93, 1114
Lützgendorf N., Kissler-Patig M., Noyola E., Jalali B., de Zeeuw P. T., Gebhardt K., Baumgardt H., 2011, A&A, 533, A36
Lützgendorf N., Kissler-Patig M., Gebhardt K., Baumgardt H., Noyola E., Jalali B., de Zeeuw P. T., Neumayer N., 2012, A&A, 542, A129
Lützgendorf N., Baumgardt H., Kruijssen J. M. D., 2013a, A&A, 558, A117
Lützgendorf N. et al., 2013b, A&A, 552, A49
Lützgendorf N., Gebhardt K., Baumgardt H., Noyola E., Neumayer N., Kissler-Patig M., de Zeeuw T., 2015, A&A, 581, A1
Maccarone T. J., Fender R. P., Tzioumis A. K., 2005, MNRAS, 356, L17
Mackey A. D., Wilkinson M. I., Davies M. B., Gilmore G. F., 2007, MNRAS, 379, L40
MacLean B. T., Campbell S. W., De Silva G. M., Lattanzio J., D'Orazi V., Simpson J. D., Momany Y., 2016, MNRAS, 460, L69
Majewski S. R. et al., 2016, Astron. Nachr., 337, 863
Malavolta L., Piotto G., Bedin L. R., Sneden C., Nascimbeni V., Sommariva V., 2015, MNRAS, 454, 2621
Manchester R. N., Lyne A. G., Robinson C., Bailes M., D'Amico N., 1991, Nature, 352, 219
Mandushev G., Staneva A., Spasova N., 1991, A&A, 252, 94
Marino A. F. et al., 2014, MNRAS, 437, 1609
Marino A. F. et al., 2015, MNRAS, 450, 815
Marino A. F. et al., 2016, MNRAS, 459, 610
Mashchenko S., Sills A., 2005, ApJ, 619, 243
Mayor M. et al., 1983, A&AS, 54, 495
Mayor M. et al., 1997, AJ, 114, 1087
McLaughlin D. E., van der Marel R. P., 2005, ApJS, 161, 304
McLaughlin D. E., Anderson J., Meylan G., Gebhardt K., Pryor C., Minniti D., Phinney S., 2006, ApJS, 166, 249
McNamara B. J., Harrison T. E., Anderson J., 2003, ApJ, 595, 187
McNamara B. J., Harrison T. E., Baumgardt H., Khalaj P., 2012, ApJ, 745, 175
Melbourne J., Sarajedini A., Layden A., Martins D. H., 2000, AJ, 120, 3127
Mészáros S., Dupree A. K., Szalai T., 2009, AJ, 137, 4282
Meylan G., Mayor M., 1991, A&A, 250, 113
Michie R. W., 1963, MNRAS, 125, 127
Milone A. P., Villanova S., Bedin L. R., Piotto G., Carraro G., Anderson J., King I. R., Zaggia S., 2006, A&A, 456, 517
Morscher M., Umbreit S., Farr W. M., Rasio F. A., 2013, ApJ, 763, L15
Mucciarelli A., Lapenna E., Massari D., Ferraro F. R., Lanzoni B., 2015, ApJ, 801, 69
Nitadori K., Aarseth S. J., 2012, MNRAS, 424, 545
Noyola E., Gebhardt K., 2006, AJ, 132, 447
Noyola E., Gebhardt K., Bergmann M., 2008, ApJ, 676, 1008
Noyola E., Gebhardt K., Kissler-Patig M., Lützgendorf N., Jalali B., de Zeeuw P. T., Baumgardt H., 2010, ApJ, 719, L60
Pancino E., Galfo A., Ferraro F. R., Bellazzini M., 2007, ApJ, 661, L155
Paust N. E. Q. et al., 2010, AJ, 139, 476
Peterson R. C., Cudworth K. M., 1994, ApJ, 420, 612
Peterson R. C., Latham D. W., 1986, ApJ, 305, 645
Peterson R. C., Seitzer P., Cudworth K. M., 1989, ApJ, 347, 251
Peterson R. C., Rees R. F., Cudworth K. M., 1995, ApJ, 443, 124
Peuten M., Zocchi A., Gieles M., Gualandris A., Henault-Brunet V., 2016, MNRAS, 462, 2333
Piatek S., Pryor C., McClure R. D., Fletcher J. M., Hesser J. E., 1994, AJ, 107, 1397
Pietrinferni A., Cassisi S., Salaris M., Castelli F., 2006, ApJ, 642, 797
Pilachowski C. A., Sneden C., Kraft R. P., Harmer D., Willmarth D., 2000, AJ, 119, 2895
Pooley D. et al., 2003, ApJ, 591, L131
Portegies Zwart S. F., McMillan S. L. W., 2002, ApJ, 576, 899
Portegies Zwart S. F., Baumgardt H., Hut P., Makino J., McMillan S. L. W., 2004, Nature, 428, 724
Pryor C., Meylan G., 1993, in Djorgovski S. G., Meylan G., eds, ASP Conf. Ser. Vol. 50, Structure and Dynamics of Globular Clusters. Astron. Soc. Pac., San Francisco, p. 357
Pryor C., Hartwick F. D. A., McClure R. D., Fletcher J. M., Kormendy J., 1986, AJ, 91, 546

Pryor C., McClure R. D., Fletcher J. M., Hesser J. E., 1991, AJ, 102, 1026
Rastorguev A. S., Samus N. N., 1991, Sov. Astron. Lett., 17, 388
Reijns R. A., Seitzer P., Arnold R., Freeman K. C., Ingerson T., van den Bosch R. C. E., van de Ven G., de Zeeuw P. T., 2006, A&A, 445, 503
Rodriguez C. L., Chatterjee S., Rasio F. A., 2016a, Phys. Rev. D, 93, 084029
Rodriguez C. L., Haster C.-J., Chatterjee S., Kalogera V., Rasio F. A., 2016b, ApJ, 824, L8
Roederer I. U., Mateo M., Bailey J. I., Spencer M., Crane J. D., Shectman S. A., 2016, MNRAS, 455, 2417
Roeser S., Demleitner M., Schilbach E., 2010, AJ, 139, 2440
Rojas-Arriagada A., Zoccali M., Vásquez S., Ripepi V., Musella I., Marconi M., Grado A., Limatola L., 2016, A&A, 587, A95
Salinas R., Jílková L., Carraro G., Catelan M., Amigo P., 2012, MNRAS, 421, 960
Sarajedini A. et al., 2007, AJ, 133, 1658
Scarpa R., Falomo R., 2010, A&A, 523, A43
Scarpa R., Marconi G., Gilmozzi R., Carraro G., 2007a, The Messenger, 128, 41
Scarpa R., Marconi G., Gilmozzi R., Carraro G., 2007b, A&A, 462, L9
Scarpa R., Marconi G., Carraro G., Falomo R., Villanova S., 2011, A&A, 525, A148
Schönebeck F., 2015, PhD Thesis, Univ. Heidelberg
Servillat M., Farrell S. A., Lin D., Godet O., Barret D., Webb N. A., 2011, ApJ, 743, 6
Shanahan R. L., Gieles M., 2015, MNRAS, 448, L94
Simmerer J., Feltzing S., Primas F., 2013, A&A, 556, A58
Smolinski J. P. et al., 2011, AJ, 141, 89
Sollima A., Bellazzini M., Smart R. L., Correnti M., Pancino E., Ferraro F. R., Romano D., 2009, MNRAS, 396, 2183
Sollima A., Bellazzini M., Lee J.-W., 2012, ApJ, 755, 156
Spitzer L., 1987, Dynamical Evolution of Globular Clusters. Princeton Univ. Press, Princeton, NJ
Strader J., Caldwell N., Seth A. C., 2011, AJ, 142, 8
Trager S. C., King I. R., Djorgovski S., 1995, AJ, 109, 218
Trenti M., van der Marel R., 2013, MNRAS, 435, 3272
Valenti E., Ferraro F. R., Origlia L., 2007, AJ, 133, 1287
van de Ven G., van den Bosch R. C. E., Verolme E. K., de Zeeuw P. T., 2006, A&A, 445, 513
van der Marel R. P., Anderson J., 2010, ApJ, 710, 1063
VandenBerg D. A., Brogaard K., Leaman R., Casagrande L., 2013, ApJ, 775, 134
Verbunt F., 1993, ARA&A, 31, 93
Villanova S., Geisler D., Gratton R. G., Cassisi S., 2014, ApJ, 791, 107
Villanova S., Monaco L., Moni Bidin C., Assmann P., 2016, MNRAS, 460, 2351
Wang L. et al., 2016a, MNRAS, 458, 1450
Wang Y., Primas F., Charbonnel C., Van der Swaelmen M., Bono G., Chantereau W., Zhao G., 2016b, A&A, 592, A66
Watkins L. L., van der Marel R. P., Bellini A., Anderson J., 2015a, ApJ, 803, 29
Watkins L. L., van der Marel R. P., Bellini A., Anderson J., 2015b, ApJ, 812, 149
Webb N. A., Barret D., Godet O., Servillat M., Farrell S. A., Oates S. R., 2010, ApJ, 712, L107
Yong D., Da Costa G. S., Norris J. E., 2016, MNRAS, 460, 1846
Zaritsky D., Colucci J. E., Pessev P. M., Bernstein R. A., Chandar R., 2014, ApJ, 796, 71
Zinn R., Barnes S., 1998, AJ, 116, 1736
Zocchi A., Gieles M., Hénault-Brunet V., 2016a, in Meiron Y., Li S., Liu F.-K., Spurzem R., eds, Proc. IAU Symp. 312, Star Clusters and Black Holes in Galaxies across Cosmic Time. p. 197
Zocchi A., Gieles M., Hénault-Brunet V., Varri A. L., 2016b, MNRAS, 462, 696

SUPPORTING INFORMATION

Additional Supporting Information may be found in the online version of this article:

(http://www.mnras.oxfordjournals.org/lookup/suppl/doi:10.1093/mnras/stw2488/-/DC1).

Please note: Oxford University Press is not responsible for the content or functionality of any supporting materials supplied by the authors. Any queries (other than missing material) should be directed to the corresponding author for the article.

APPENDIX A: SOURCES FOR THE PHOTOMETRIC AND SPECTROSCOPIC INFORMATION OF INDIVIDUAL CLUSTERS

Table A1. Sources for velocity and surface density data used in this work (LOS = line-of-sight radial velocities, PM = proper motion velocity dispersion profile, IFU = Integral field unit velocity dispersion, SD = surface density profile).

Name	Source	Type
NGC 104	Mayor et al. (1983)	LOS
	Gebhardt et al. (1995)	LOS
	McLaughlin et al. (2006)	PM
	Carretta et al. (2009b)	LOS
	Lane et al. (2011)	LOS
	Gratton et al. (2013)	LOS
	Watkins et al. (2015a)	PM
	Da Costa (2016)	LOS
	Marino et al. (2016)	LOS
NGC 288	Pryor et al. (1991)	LOS
	Lane et al. (2011)	LOS
	Lucatello et al. (2015)	LOS
	Watkins et al. (2015a)	PM
	Da Costa (2016)	LOS
NGC 362	Fischer et al. (1993)	LOS
	Carretta et al. (2013)	LOS
	D'Orazi et al. (2015)	LOS
	Schönebeck (2015)	LOS
	Watkins et al. (2015a)	PM
NGC 1851	Scarpa et al. (2011)	LOS
	Gratton et al. (2012)	LOS
	Lützgendorf et al. (2013)	IFU
	Lardo et al. (2015)	LOS
	Lucatello et al. (2015)	LOS
	Watkins et al. (2015a)	PM, LOS
NGC 1904	Carretta et al. (2009b)	LOS
	Scarpa et al. (2011)	LOS
	Lützgendorf et al. (2013)	IFU
	D'Orazi et al. (2015)	LOS
NGC 2419	Baumgardt et al. (2009)	LOS
	Ibata et al. (2011)	LOS
	Bellazzini (2007)	SD
NGC 2808	Cacciari et al. (2004)	LOS
	Carretta et al. (2006)	LOS
	Gratton et al. (2011)	LOS
	Lützgendorf et al. (2012)	IFU, LOS
	Marino et al. (2014)	LOS
	Lardo et al. (2015)	LOS
	D'Orazi et al. (2015)	LOS
	Wang et al. (2016b)	LOS
	Watkins et al. (2015a)	PM, LOS
NGC 3201	Cote et al. (1995)	LOS
	Carretta et al. (2009b)	LOS
	Mucciarelli et al. (2015)	LOS
NGC 4147	Kimmig et al. (2015)	LOS
	Villanova et al. (2016)	LOS
NGC 4372	Kacharov et al. (2014)	LOS, SD
	Lardo et al. (2015)	LOS
NGC 4590	Carretta et al. (2009b)	LOS
	Lane et al. (2011)	LOS
NGC 4833	Carretta et al. (2014a)	LOS
	Lardo et al. (2015)	LOS
	Melbourne et al. (2000)	SD
NGC 5024	Lane et al. (2011)	LOS
	Kimmig et al. (2015)	LOS
NGC 5053	Boberg, Friel & Vesperini (2015)	LOS
	Kimmig et al. (2015)	LOS
NGC 5139	Mayor et al. (1997)	LOS
	Reijns et al. (2006)	LOS
	van de Ven et al. (2006)	PM
	Pancino et al. (2007)	LOS
	Johnson et al. (2008)	LOS
	Sollima et al. (2009)	LOS
	Noyola et al. (2010)	IFU
	Scarpa & Falomo (2010)	LOS
	Da Costa (2012)	LOS
	Villanova et al. (2014)	LOS
	Watkins et al. (2015a)	PM
	Gebhardt (private communication)	LOS
NGC 5272	Gunn & Griffin (1979)	LOS
	Pilachowski et al. (2000)	LOS
	Smolinski et al. (2011)	LOS
	Kamann et al. (2014)	LOS
	Kimmig et al. (2015)	LOS
NGC 5286	Feldmeier et al. (2013)	IFU, LOS, SD
	Marino et al. (2015)	LOS
NGC 5466	Pryor et al. (1991)	LOS
	Kimmig et al. (2015)	LOS
NGC 5694	Lützgendorf et al. (2013)	IFU, SD
	Bellazzini et al. (2015)	LOS
NGC 5824	Lützgendorf et al. (2013)	IFU, SD
	Roederer et al. (2016)	LOS
NGC 5904	Rastorguev & Samus (1991)	LOS
	Battaglia et al. (2008)	LOS
	Carretta et al. (2009b)	LOS
	Gratton et al. (2013)	LOS
	Kimmig et al. (2015)	LOS
	Watkins et al. (2015a)	PM
NGC 5927	Simmerer, Feltzing & Primas (2013)	LOS
	Lardo et al. (2015)	LOS
	Watkins et al. (2015a)	PM
NGC 6093	Lützgendorf et al. (2013)	IFU, LOS, SD
	Carretta et al. (2015)	LOS
NGC 6121	Peterson, Rees & Cudworth (1995)	LOS
	Ivans et al. (1999)	LOS
	Carretta et al. (2009b)	LOS
	Lane et al. (2011)	LOS
	Malavolta et al. (2015)	LOS
	MacLean et al. (2016)	LOS
NGC 6139	Bragaglia et al. (2015)	LOS
NGC 6171	Piatek et al. (1994)	LOS
	Scarpa et al. (2007a)	LOS
	Carretta et al. (2009b)	LOS
NGC 6205	Lupton, Gunn & Griffin (1987)	LOS
	Pilachowski et al. (2000)	LOS
	Lee et al. (2008)	LOS
	Mészáros, Dupree & Szalai (2009)	LOS
	Smolinski et al. (2011)	LOS
	Kamann et al. (2014)	LOS
NGC 6218	Carretta et al. (2007a)	LOS
	Lane et al. (2011)	LOS
NGC 6254	Carretta et al. (2009b)	LOS
NGC 6266	McNamara et al. (2012)	PM
	Lützgendorf et al. (2013)	IFU
	Watkins et al. (2015a)	PM
NGC 6273	Johnson et al. (2015)	LOS
	Yong, Da Costa & Norris (2016)	LOS
NGC 6341	Pilachowski et al. (2000)	LOS
	Drukier et al. (2007)	LOS
	Mészáros et al. (2009)	LOS
	Kamann et al. (2014)	LOS
	Kimmig et al. (2015)	LOS
	Watkins et al. (2015a)	PM
NGC 6362	Watkins et al. (2015a)	PM
NGC 6388	Carretta et al. (2009b)	LOS

Table A1. *– continued*

Name	Source	Type
	Lanzoni et al. (2013)	LOS
	Lützgendorf et al. (2013)	IFU, SD
	Lapenna et al. (2015)	LOS
	Watkins et al. (2015a)	PM
NGC 6397	Meylan & Mayor (1991)	LOS
	Gebhardt et al. (1995)	LOS
	Milone et al. (2006)	LOS
	Carretta et al. (2009b)	LOS
	Lind et al. (2009)	LOS
	Lovisi et al. (2012)	LOS
	Kamann et al. (2016)	LOS
	Watkins et al. (2015a)	PM
NGC 6402	Kimmig et al. (2015)	LOS
NGC 6441	Watkins et al. (2015a)	PM
NGC 6535	Zaritsky et al. (2014)	LOS
	Watkins et al. (2015a)	PM
NGC 6624	Watkins et al. (2015a)	PM
NGC 6656	Peterson & Cudworth (1994)	LOS
	Cote et al. (1996)	LOS
	Lane et al. (2011)	LOS
	Gratton et al. (2014)	LOS
	Watkins et al. (2015a)	PM
NGC 6681	Watkins et al. (2015a)	PM
NGC 6715	Bellazzini et al. (2008)	LOS
	Ibata et al. (2009)	LOS
	Carretta et al. (2010)	LOS
	Watkins et al. (2015a)	PM
NGC 6723	Rojas-Arriagada et al. (2016)	LOS
	Gratton et al. (2015)	LOS
NGC 6752	Carretta et al. (2007b)	LOS
	Lane et al. (2011)	LOS
	Lovisi et al. (2013)	LOS
	Lardo et al. (2015)	LOS
	Watkins et al. (2015a)	PM
NGC 6809	Carretta et al. (2009b)	LOS
	Lane et al. (2011)	LOS
NGC 6838	Peterson & Latham (1986)	LOS
	Carretta et al. (2009b)	LOS
	Smolinski et al. (2011)	LOS
	Kimmig et al. (2015)	LOS
	Cordero et al. (2015)	LOS
	Drukier, Fahlman & Richer (1992)	SD
NGC 7078	Peterson, Seitzer & Cudworth (1989)	LOS
	Drukier et al. (1998)	LOS
	Gebhardt et al. (2000)	LOS
	Gerssen et al. (2002)	LOS
	Carretta et al. (2009b)	LOS
	Lardo et al. (2015)	LOS
	Kimmig et al. (2015)	LOS
	McNamara, Harrison & Anderson (2003)	PM
	Watkins et al. (2015a)	PM
NGC 7089	Pryor et al. (1986)	LOS
	Lee et al. (2008)	LOS
	Schönebeck (2015)	LOS
	Kimmig et al. (2015)	LOS
NGC 7099	Gebhardt et al. (1995)	LOS
	Scarpa et al. (2007b)	LOS
	Carretta et al. (2009b)	LOS
	Lane et al. (2011)	LOS
Terzan 8	Carretta et al. (2014b)	LOS
	Salinas et al. (2012)	SD

APPENDIX B: FITS OF THE SURFACE DENSITY AND VELOCITY DISPERSION PROFILES OF INDIVIDUAL CLUSTERS

Figs B1–B13 depict our fits of the observed surface density and velocity dispersion profiles for all studied clusters. The surface densities in the left-hand panels are normalized to 1. In the right-hand panels, the proper motion data are shown by orange circles while the radial velocity dispersion profiles derived in this work are shown by blue circles. The predictions of the best-fitting *N*-body models are shown as solid, red lines. For clarity we show only the radial velocity dispersion profiles. The proper motion velocity dispersion profiles are only a few per cent higher due to mass segregation. The *N*-body models shown are the best-fitting no-IMBH models except for NGC 5139 and NGC 6715, which show the best-fitting IMBH models.

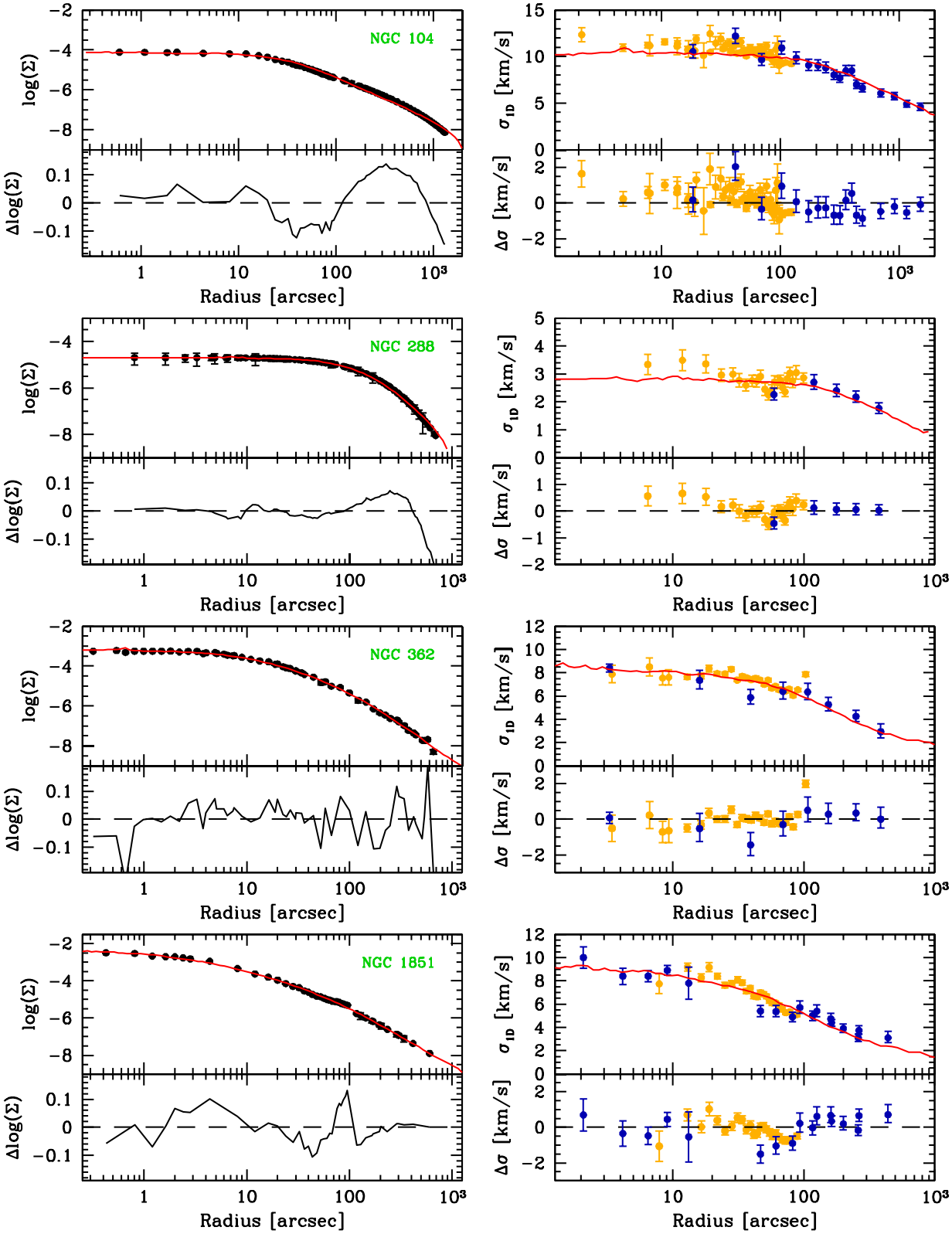

Figure B1. Fit of the surface density profiles (left-hand panels) and velocity dispersion profiles (right-hand panels) for NGC 104, NGC 288, NGC 362 and NGC 1851. The surface densities in the left-hand panels are normalized to 1. In the right-hand panels, the observed proper motion velocity dispersion profile is shown by orange circles while the radial velocity dispersion profile derived in this work is shown by blue circles. Red curves show the surface density (left-hand panel) and line-of-sight velocity dispersion (right-hand panel) of the best-fitting *N*-body model without an IMBH for each cluster. The *N*-body data provide an excellent fit to the observed data for the depicted clusters. The lower panels show the differences between the observed data and the *N*-body models.

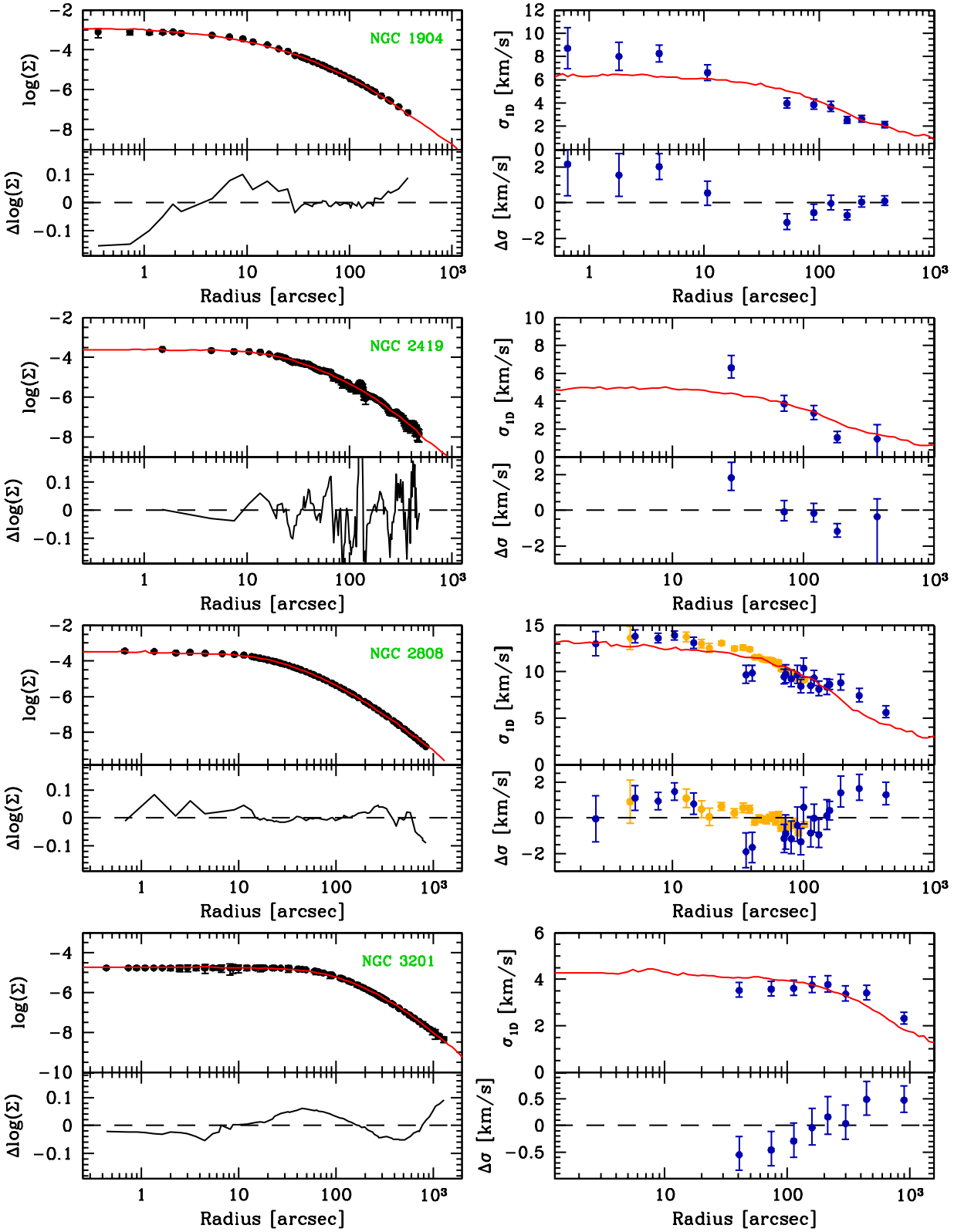

Figure B2. Same as Fig. B1 but for NGC 1904, NGC 2419, NGC 2808 and NGC 3201.

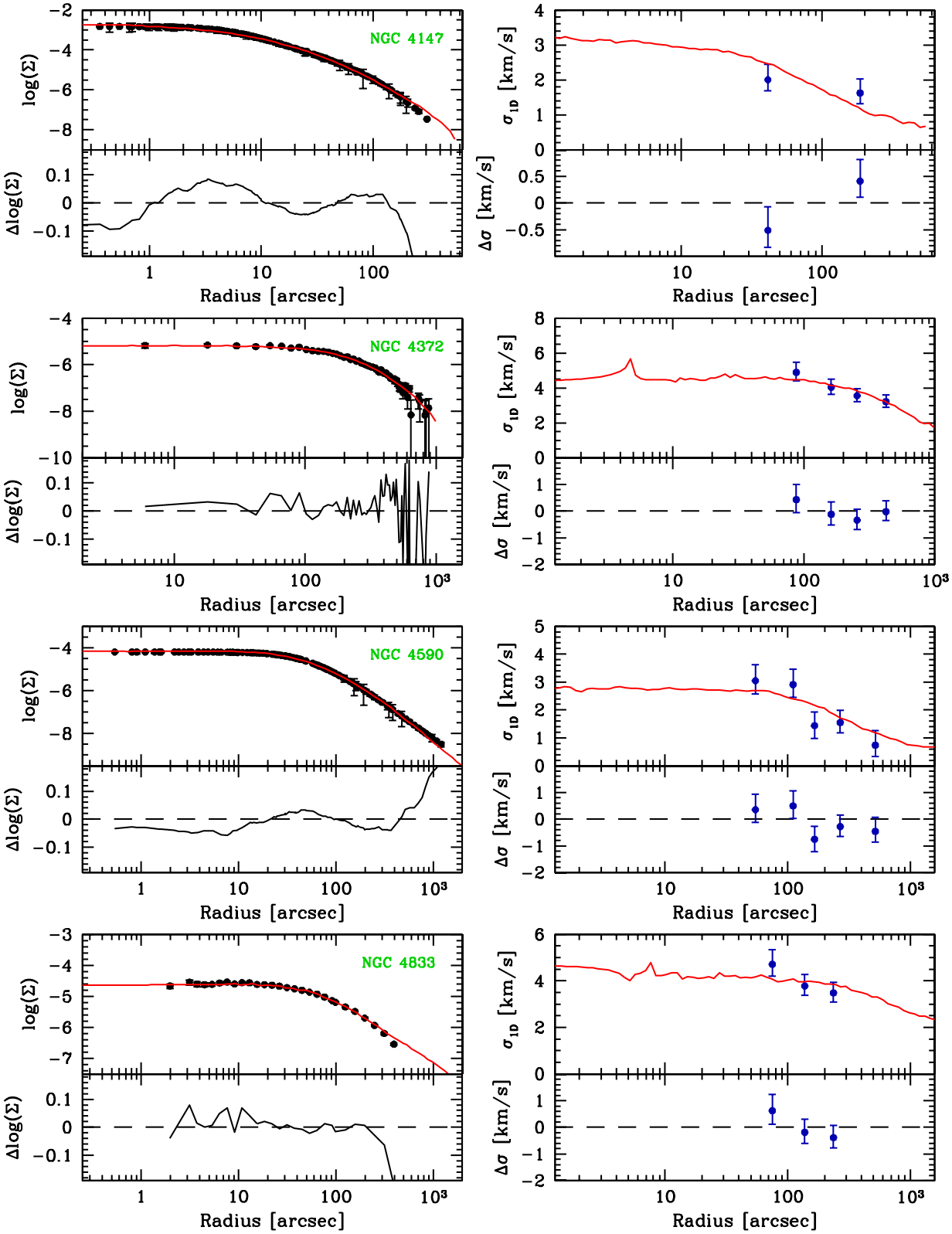

Figure B3. Same as Fig. B1 but for NGC 4147, NGC 4372, NGC 4590 and NGC 4833.

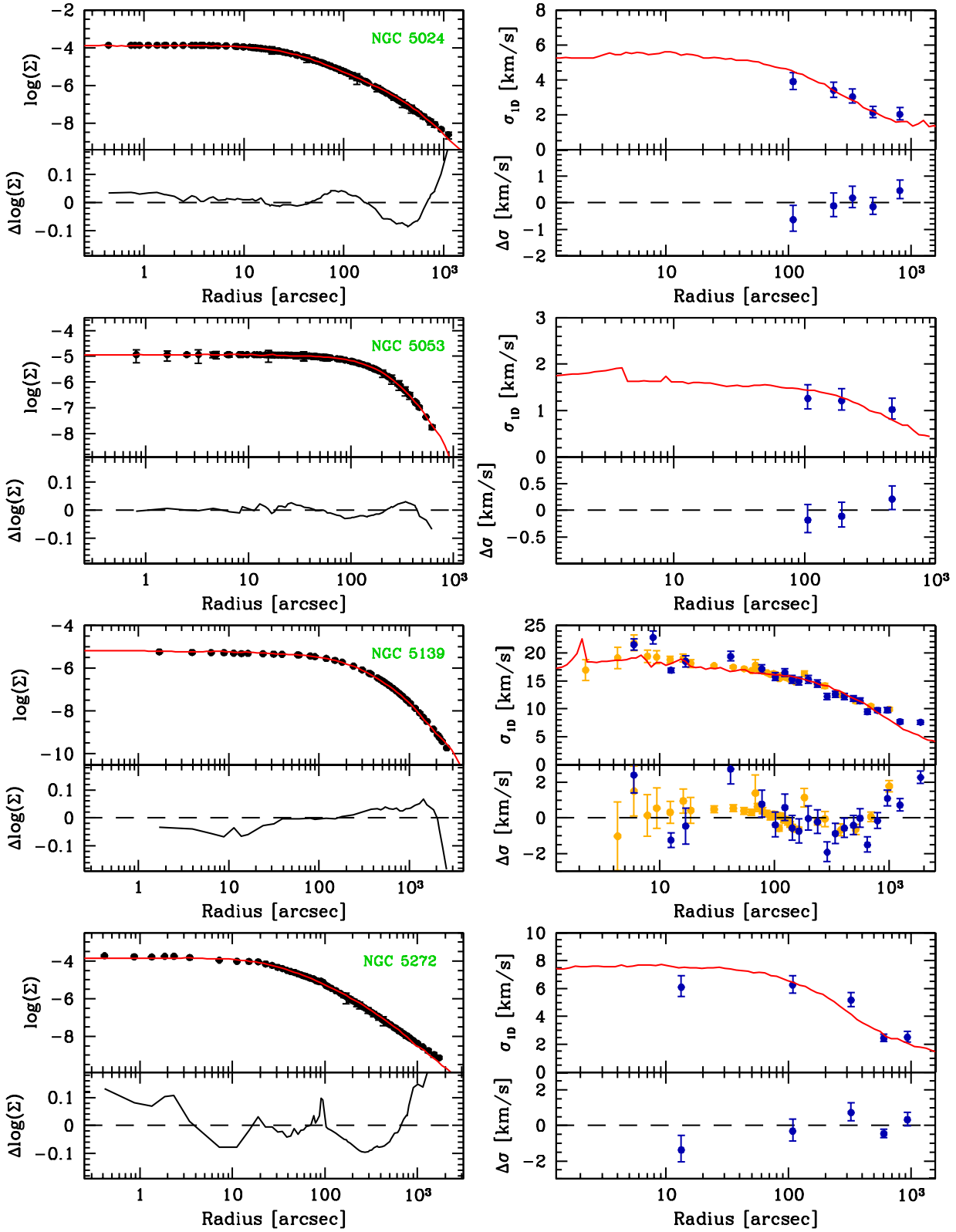

Figure B4. Same as Fig. B1 but for NGC 5024, NGC 5053, NGC 5139 and NGC 5272. The red, solid lines for NGC 5139 show the best-fitting IMBH model.

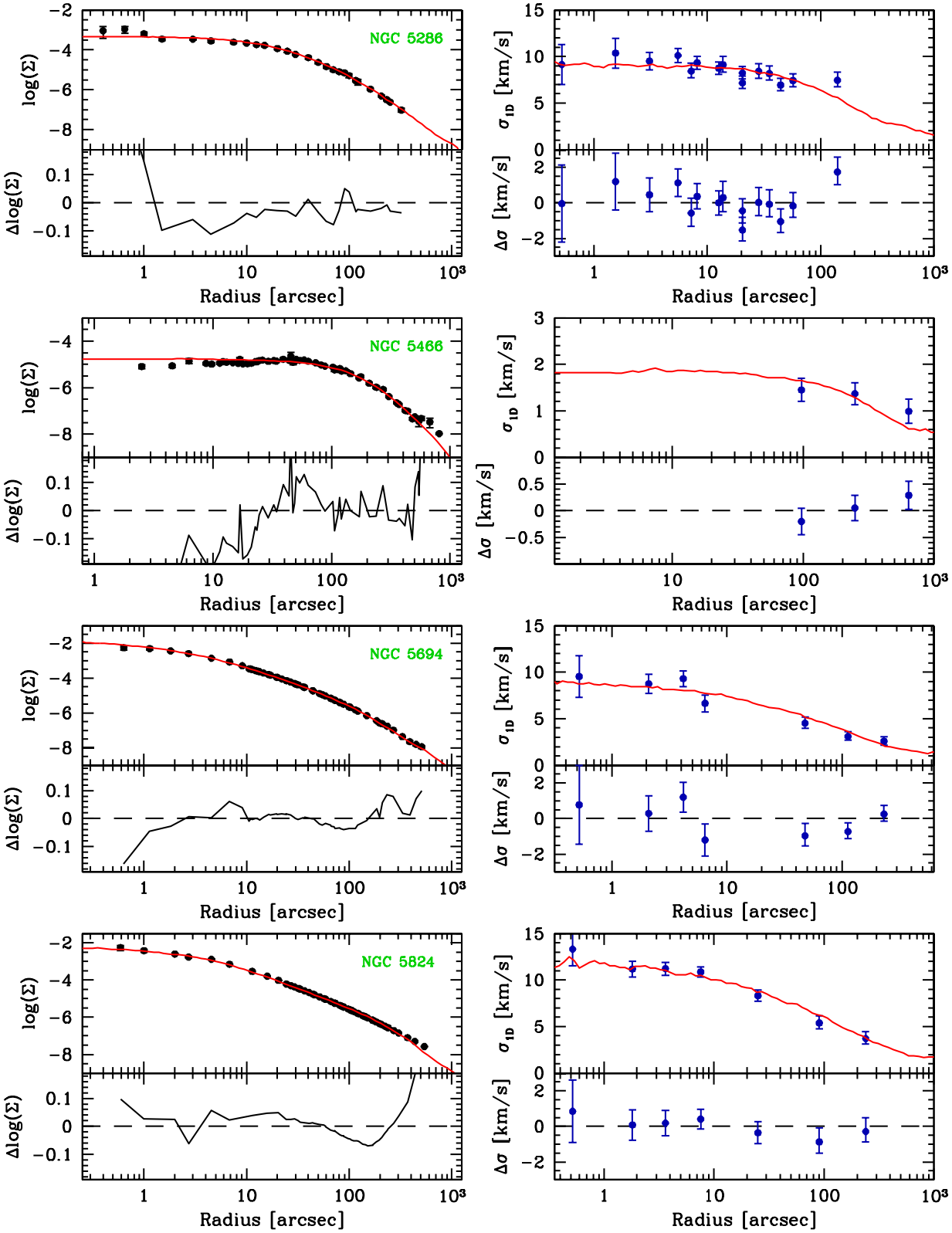

Figure B5. Same as Fig. B1 but for NGC 5286, NGC 5466, NGC 5694 and NGC 5824.

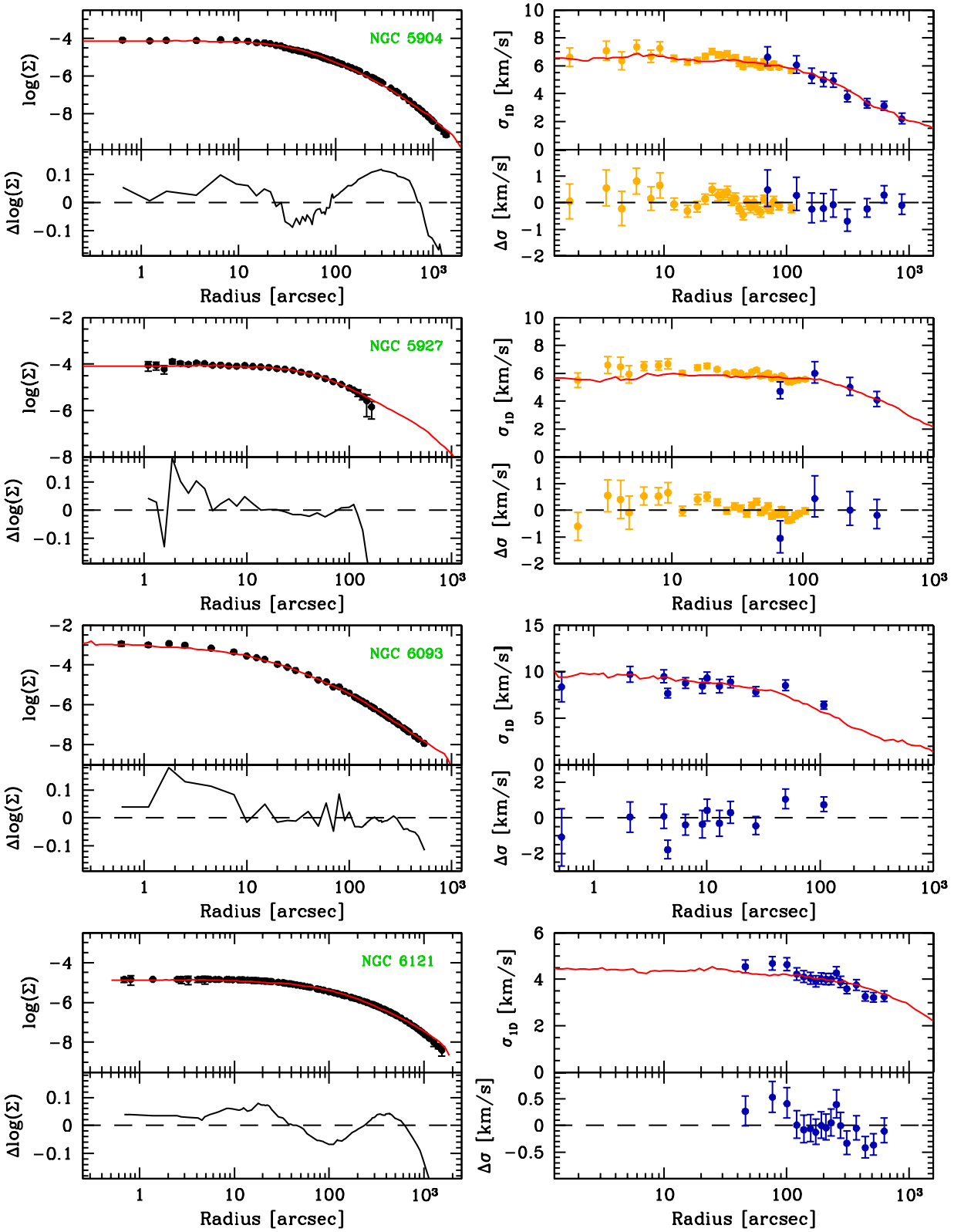

Figure B6. Same as Fig. B1 but for NGC 5904, NGC 5927, NGC 6093 and NGC 6121.

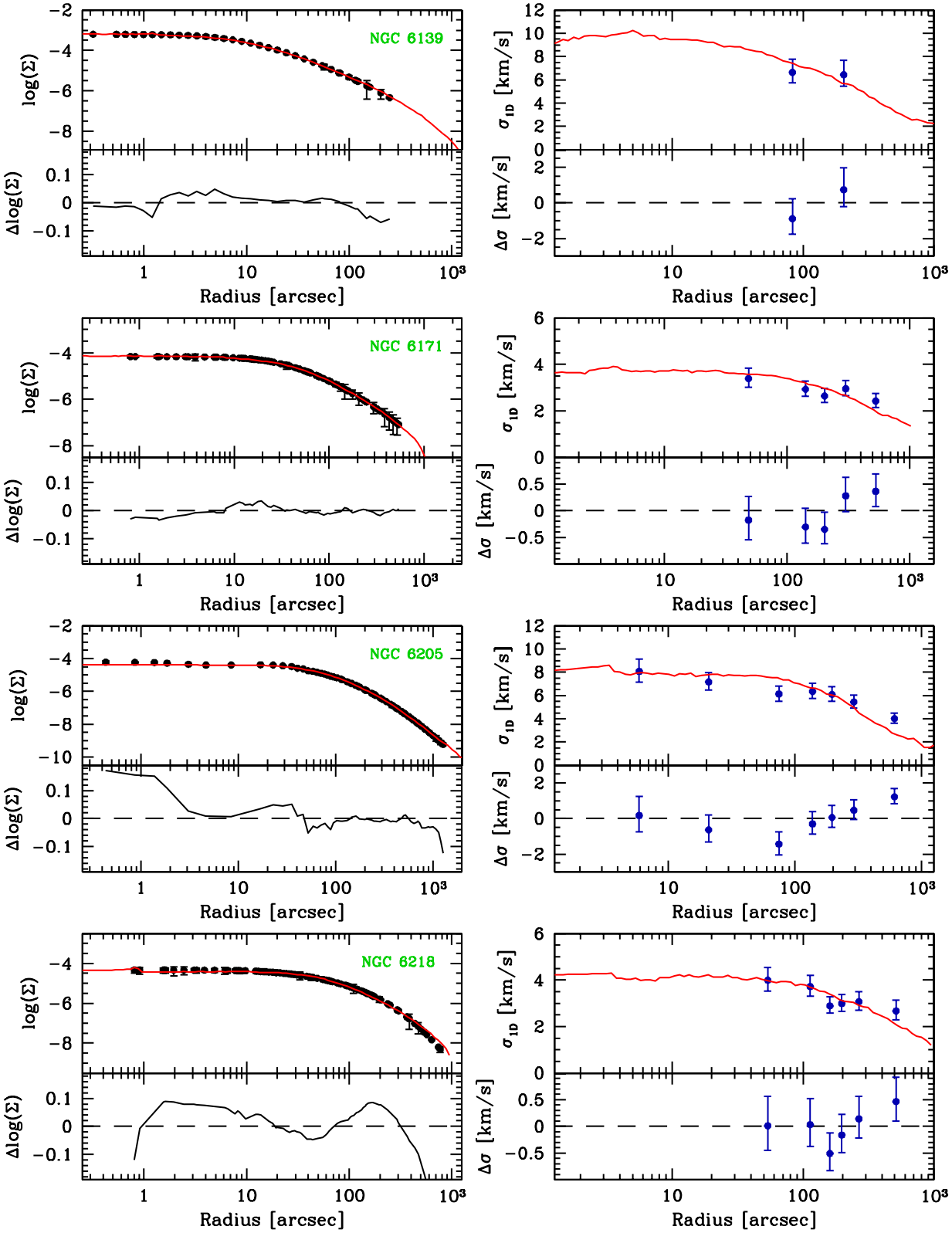

Figure B7. Same as Fig. B1 but for NGC6139, NGC 6171, NGC 6205, and NGC 6218.

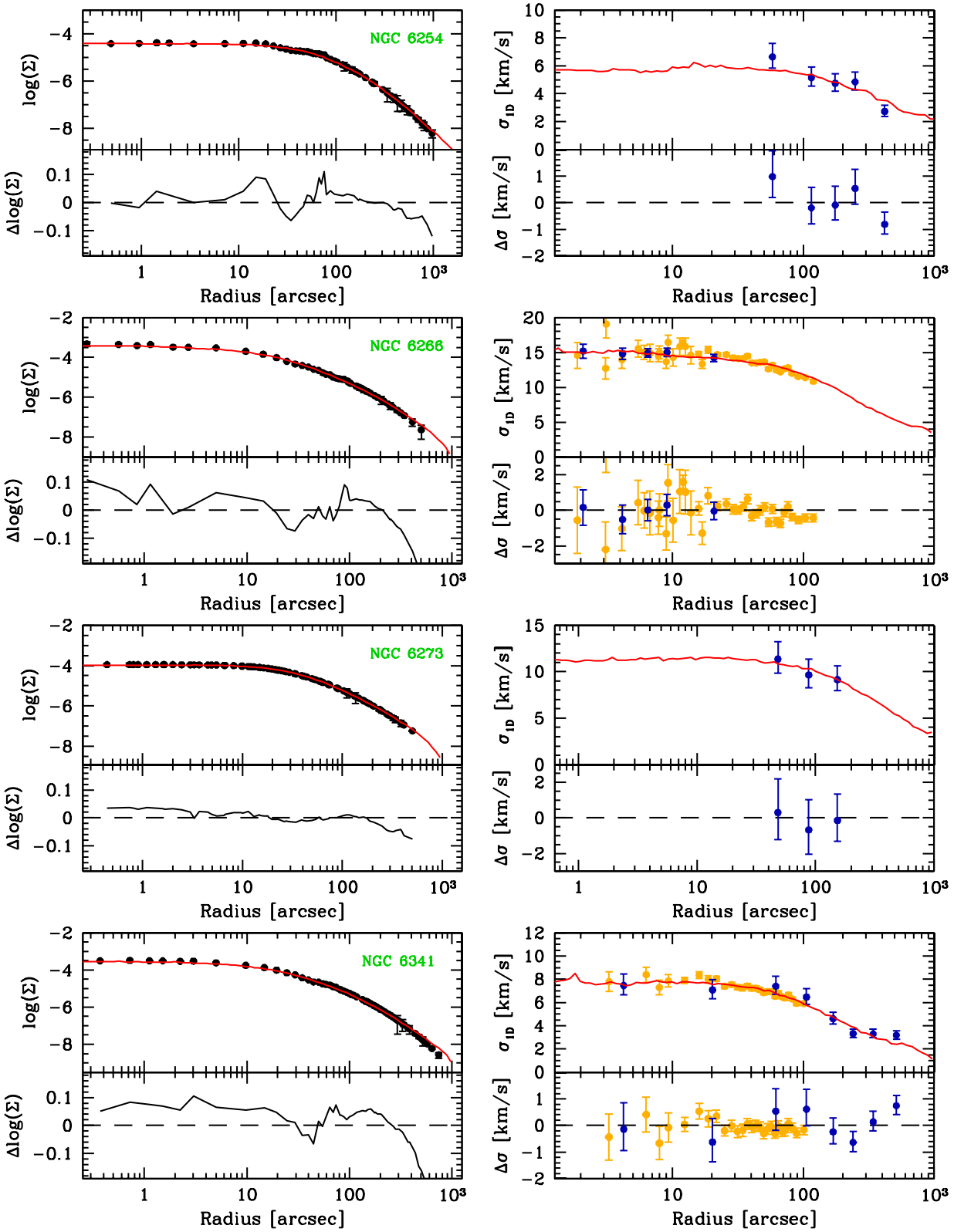

Figure B8. Same as Fig. B1 but for NGC 6254, NGC 6266, NGC 6273 and NGC 6341.

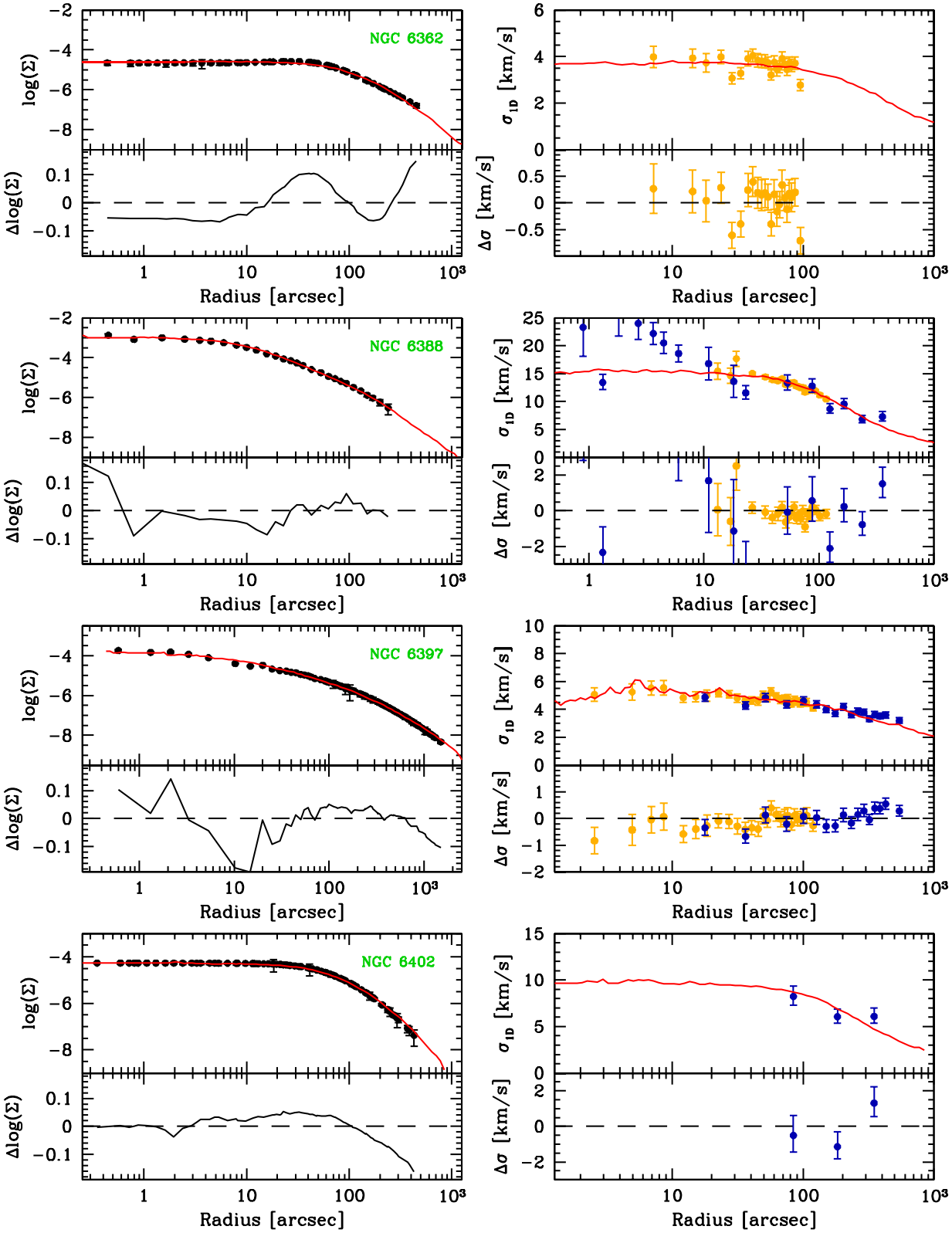

Figure B9. Same as Fig. B1 but for NGC 6362, NGC 6388, NGC 6397 and NGC 6402.

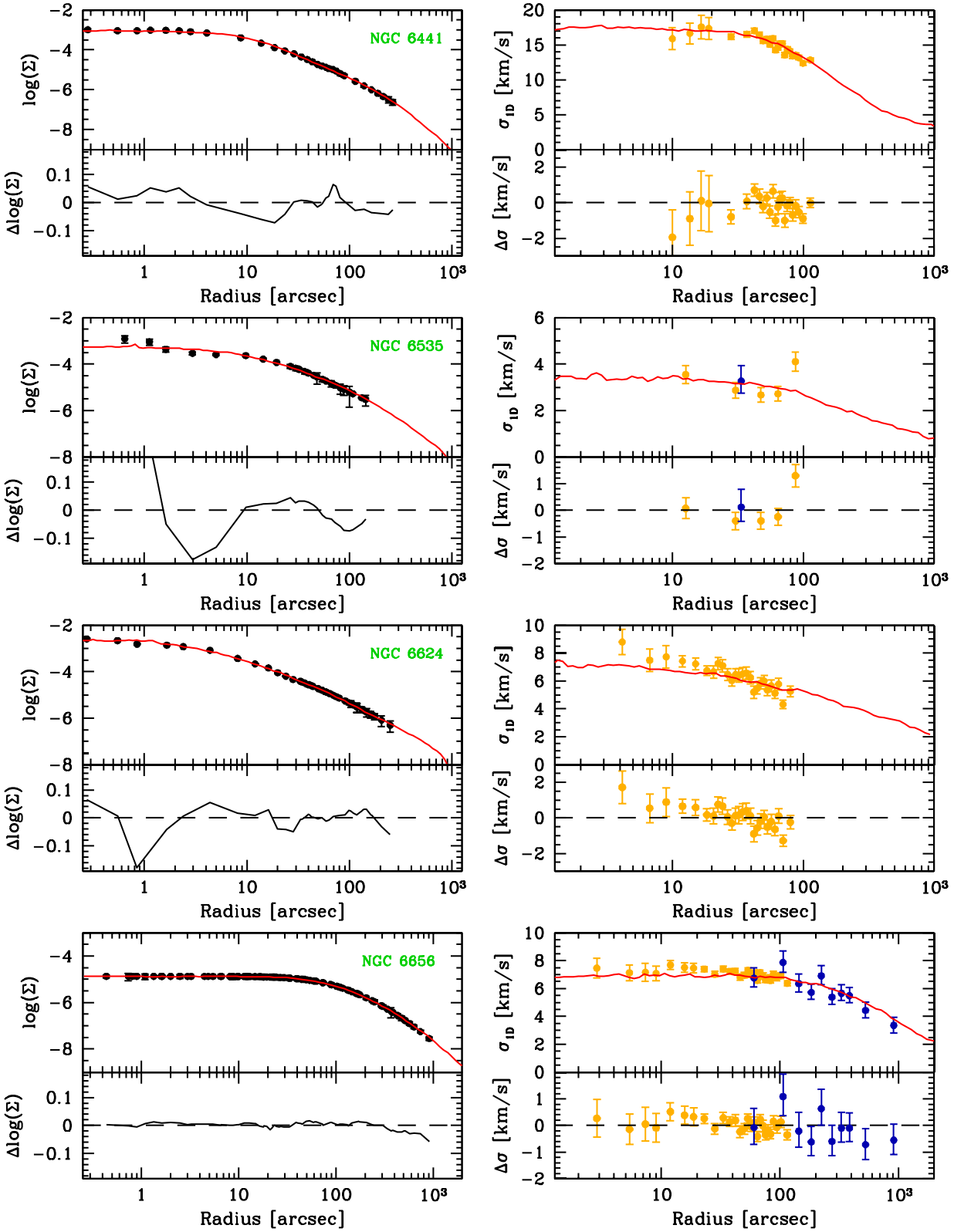

Figure B10. Same as Fig. B1 but for NGC 6441, NGC 6535, NGC 6624 and NGC 6656.

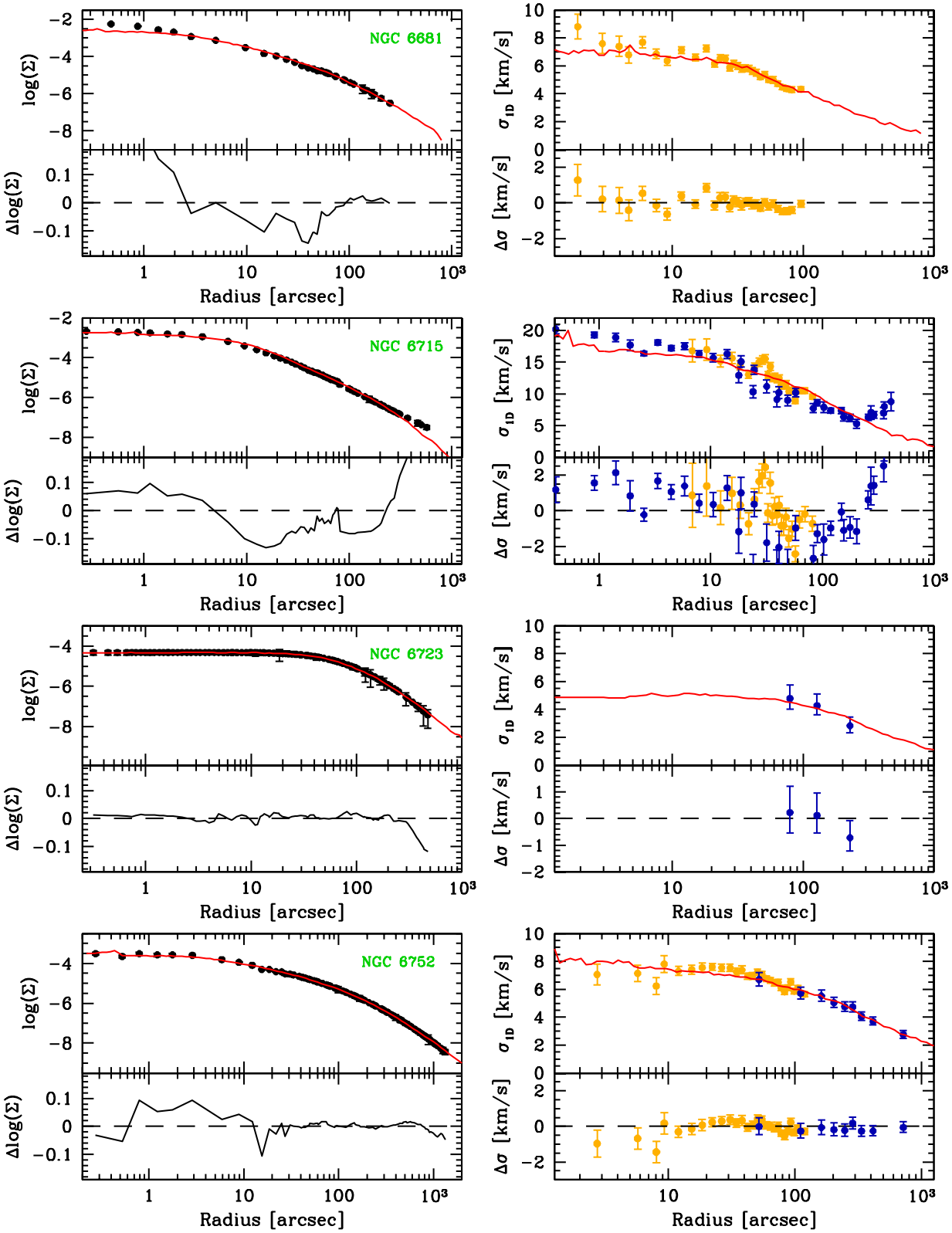

Figure B11. Same as Fig. B1 but for NGC6681, NGC 6715, NGC 6723 and NGC 6752. The red, solid lines for NGC 6715 show the best-fitting IMBH model.

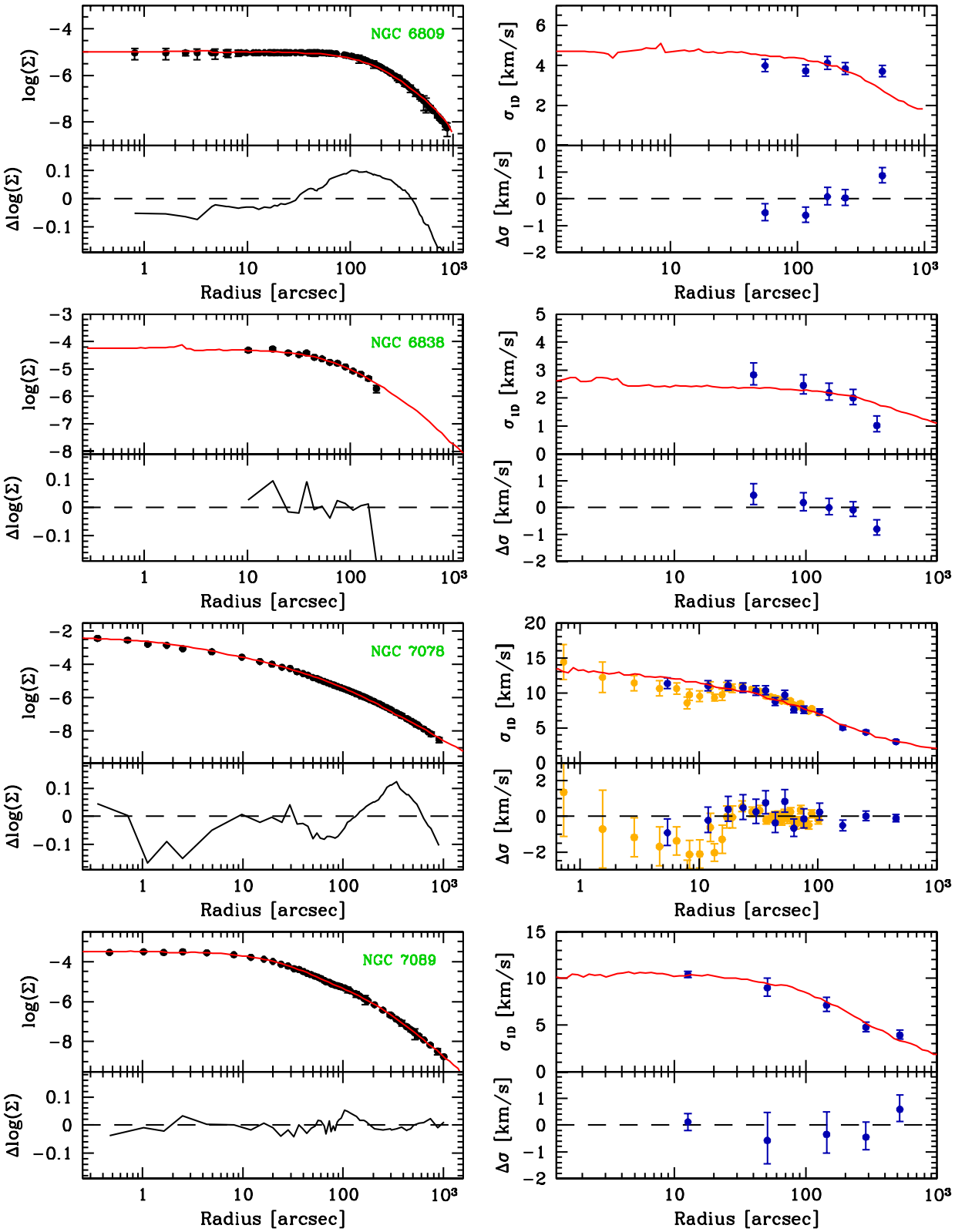

Figure B12. Same as Fig. B1 but for NGC 6809, NGC 6838, NGC 7078 and NGC 7089.

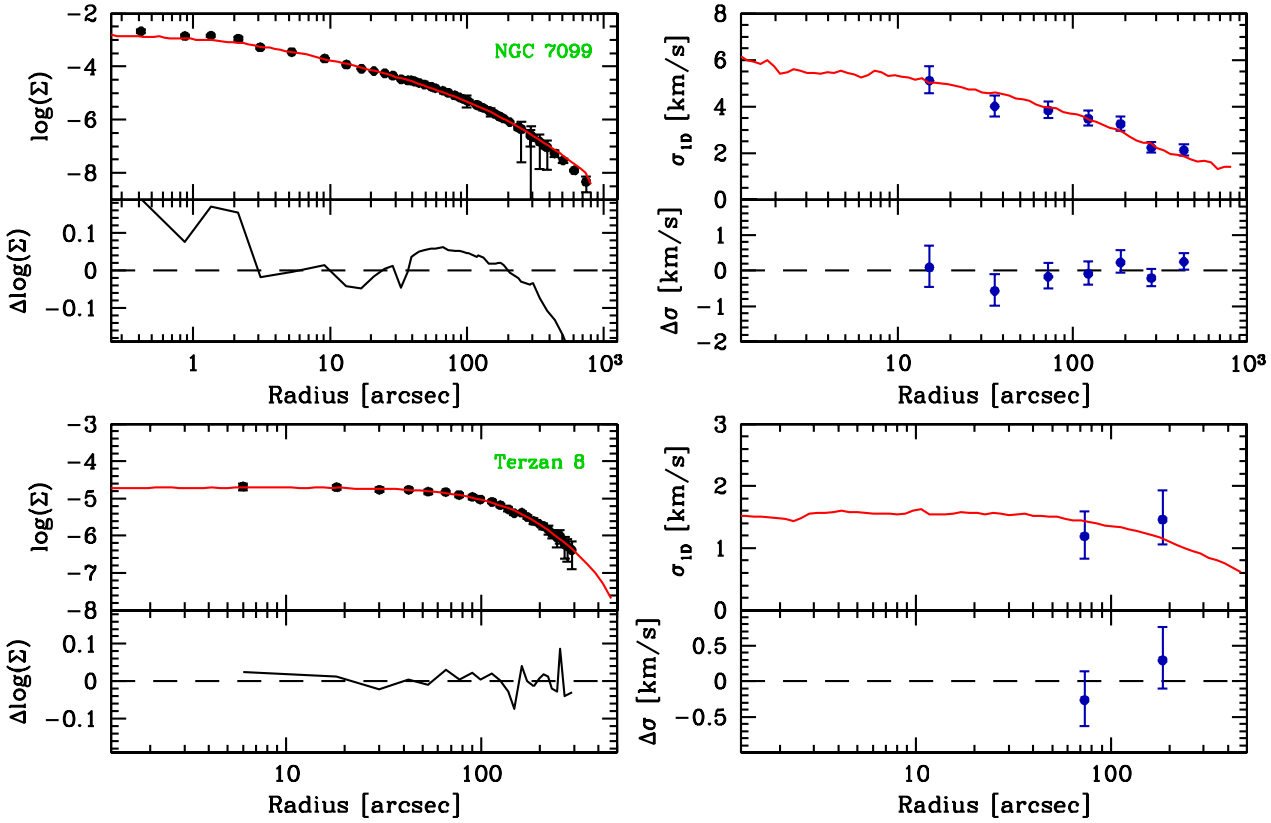

Figure B13. Same as Fig. B1 but for NGC 7099 and Terzan 8.

This paper has been typeset from a TEX/LATEX file prepared by the author.